Quaternary Science Reviews 337 (2024) 108807

Contents lists available at ScienceDirect

Quaternary Science Reviews

journal homepage: www.elsevier.com/locate/quascirev

Vegetation and precipitation change inferred from the $\delta^{13}C$ and $\delta^{2}H$ values of *n*-alkanes from lake sediment from 18 cal ka BP, tropical NE Australia

Ting Li [a,b,c,*], Youping Zhou [d,e], Chris M. Wurster [a,b,1], Xiuwen Zhou [d], Yu Zhao [e], Rainy Comley [a,b], Niels C. Munksgaard [a,b], Lucas A. Cernusak [a], Jordahna Haig [a], Michael I. Bird [a,b]

[a] College of Science and Engineering, James Cook University, Cairns, 4878, Australia
[b] ARC Centre of Excellence for Australian Biodiversity and Heritage, James Cook University, Cairns, 4878, Australia
[c] School of Earth Sciences and Resources, China University of Geosciences (Beijing), Beijing, 100083, China
[d] Isotopomics in Chemical & Biological Oceanography (ICBO), Department of Ocean Science & Engineering, Southern University of Science & Technology, Shenzhen, 518055, China
[e] Isotopomics in Chemical Biology (ICB), School of Chemistry & Chemical Engineering, Shaanxi University of Science & Technology, Xi'an, 710021, China

ARTICLE INFO

Handling editor: P Rioual

Keywords:
Paleoenvironment
n-Alkanes
Carbon and hydrogen isotopes
Lake sediment
Tropical NE Australia

ABSTRACT

The carbon and hydrogen isotope compositions ($\delta^{13}C$ and $\delta^{2}H$) of sedimentary *n*-alkanes are excellent recorders of past vegetation and precipitation change. Yet, few studies have combined and compared *n*-alkanes in modern plants and paleoenvironmental records. Here we analyzed the $\delta^{13}C$ and $\delta^{2}H$ values of *n*-alkanes ($\delta^{13}C_{alk}$ and $\delta^{2}H_{alk}$, respectively) from a 7-m-long sediment sequence in Lake Barrine, modern catchment soils, fallen leaf mixtures, rainforest tree leaves and grasses from tropical northeastern Australia. We exploited the correlation between the relative abundances, $\delta^{13}C$, and $\delta^{2}H$ values of *n*-alkanes from fresh modern rainforest leaves, grasses, fallen leaves, soils and surface sediments. Based on this, we developed two binary mixing models to determine C_3 plant abundances and the $\delta^{2}H$ values of precipitation ($\delta^{2}H_{P\text{-}R}$) to study rainfall and vegetation in the Lake Barrine catchment since 18.3 cal ka BP. Combining the results of this study with mean annual air temperature, pollen, and clastic influx, we reconstructed a robust climatic and environmental record for this site and compared it with other regional paleoenvironmental records. The modern samples indicate slight ^{13}C enrichment and obvious ^{2}H depletion in the *n*-alkanes from fresh rainforest leaves, fallen leaves, soils, and surface sediments, which is possibly due to microbial build-up of *n*-alkanes during decomposition. A broad consistency in regional paleoclimate trends was identified, including a cool, dry Last Glacial Maximum (23–17.0 cal ka BP), warmer, wetter last deglacial (17.0–14.9 cal ka BP), wetter with stable temperature Antarctic cold reversal (14.9–12.8 cal ka BP), (possibly) cooler, drier Younger Dryas (12.8–11.6 cal ka BP), warmer, wetter early-to-middle Holocene (11.6–5 cal ka BP) and cooler, slightly drier and more variable late Holocene (5 cal ka BP to the present).

1. Introduction

The carbon ($\delta^{13}C$) and hydrogen ($\delta^{2}H$) isotope compositions of plant waxes record vegetation and hydroclimatic conditions at present and in the past (Hayes et al., 1990; Bird et al., 1995; Sessions et al., 1999; Sachse et al., 2012; Liu et al., 2022). Plant waxes impregnate and cover plant cuticles, forming a continuous extracellular membrane covering the organs of lower and higher plants (Eglinton and Hamilton, 1967; Koch and Ensikat, 2008). This waxy covering prevents uncontrolled water loss by transpiration (Schönherr, 1982), and leakage of essential solutes from plants (Schönherr, 2000; Koch and Ensikat, 2008). Alkanes, alkanoic acids, alcohols, aldehydes and esters are the major components of plant waxes (Eglinton and Hamilton, 1967; Jetter et al., 2000). Long-chain *n*-alkanes ($>C_{27}$) can be well-preserved in sediments and therefore have been extensively used to reconstruct terrestrial vegetation and hydrology at present and in the geologic past (Sachse et al., 2004; Niedermeyer et al., 2014).

Compound-specific carbon isotope analysis of *n*-alkanes ($\delta^{13}C_{alk}$) in

* Corresponding author. College of Science and Engineering, James Cook University, Cairns, 4878, Australia.
E-mail address: ting.li2@my.jcu.edu.au (T. Li).
[1] Current address: Analytical Laboratories, Ruakura Research Centre, Private Bag 3345, Hamilton 3240, New Zealand.

https://doi.org/10.1016/j.quascirev.2024.108807
Received 9 May 2024; Received in revised form 28 June 2024; Accepted 28 June 2024
Available online 4 July 2024

sediments in tropical environments can help reconstruct relative contributions of C_3 and C_4 vegetation in the past (Hayes et al., 1990; Bird et al., 1995; Diefendorf et al., 2015). The $\delta^{13}C_{alk}$ values of plants are influenced by both biochemical (e.g., photosynthetic pathways) and geo-environmental factors (e.g., water availability, temperature, light intensity, altitude and latitude) (Farquhar et al., 1989; Vogts et al., 2009; Diefendorf et al., 2010; Liu and An, 2020). Photosynthetic pathways exert the strongest influence among these factors, with waxes produced by plants using the C_3 carbon fixation pathway (Calvin-Benson) significantly more ^{13}C-depleted relative to those from plants that use the C_4 carbon fixation pathway (Hatch-Slack) (O'Leary, 1981). The third photosynthetic pathway, Crassulacean acid metabolism (CAM), is less considered as only ~7% of vascular plants use this pathway (Winter and Smith, 1996).

C_3 plants include trees, shrubs and cool-climate grasses (Huang et al., 2000), with a global carbon isotope composition range of −45.9‰ to −26.9‰ for the C_{31} *n*-alkane ($\delta^{13}C_{n\text{-}C31}$) (Liu and An, 2020). C_4 plants consist mainly of tropical grasses and sedges (Huang et al., 2000), with $\delta^{13}C_{n\text{-}C31}$ values ranging from −28.5‰ to −16.7‰ globally (Liu and An, 2020). The global mean $\delta^{13}C_{n\text{-}C31}$ values for C_3 and C_4 plants are −35.4 ± 3.1‰ and −21.8 ± 2.3‰, respectively, and are markedly consistent across climate zones where they co-occur (Liu et al., 2022). Therefore, the $\delta^{13}C$ values of long chain *n*-alkanes provide a valuable proxy for the relative abundances of tropical C_3 and C_4 vegetation, provided they are terrestrially sourced, in turn providing information on climate (Ruiz Pessenda et al., 2009; Russell et al., 2014; Bird et al., 2019).

The hydrogen isotope composition of *n*-alkanes (δ^2H_{alk}) is mainly controlled by three factors: source water isotope composition, biosynthesis, and evapotranspiration, with the first being the dominant controlling factor (Sachse et al., 2012; Liu and An, 2018). Long-chain *n*-alkanes extracted from lake sediments exhibit δ^2H values that are lower than, but highly correlated with, those values of mean annual precipitation (Sachse et al., 2004; Garcin et al., 2012). Nevertheless, different net fractionations ($\varepsilon_{alk\text{-}p}$) between δ^2H_{alk} values and precipitation have been shown between monocots and dicots (Liu and An, 2019) which compose 98.2% and 77.3% of C_4 and C_3 plants, respectively (Liu and An, 2020), potentially due to different physiologies (Sachse et al., 2012; Liu et al., 2022). Therefore, major variations in plant types can impact the δ^2H values of precipitation reconstructed from δ^2H_{alk} values, which requires correction.

In tropical northern Queensland, grasses are composed of 90% or more C_4 plants (Hattersley, 1983), which means that in this region

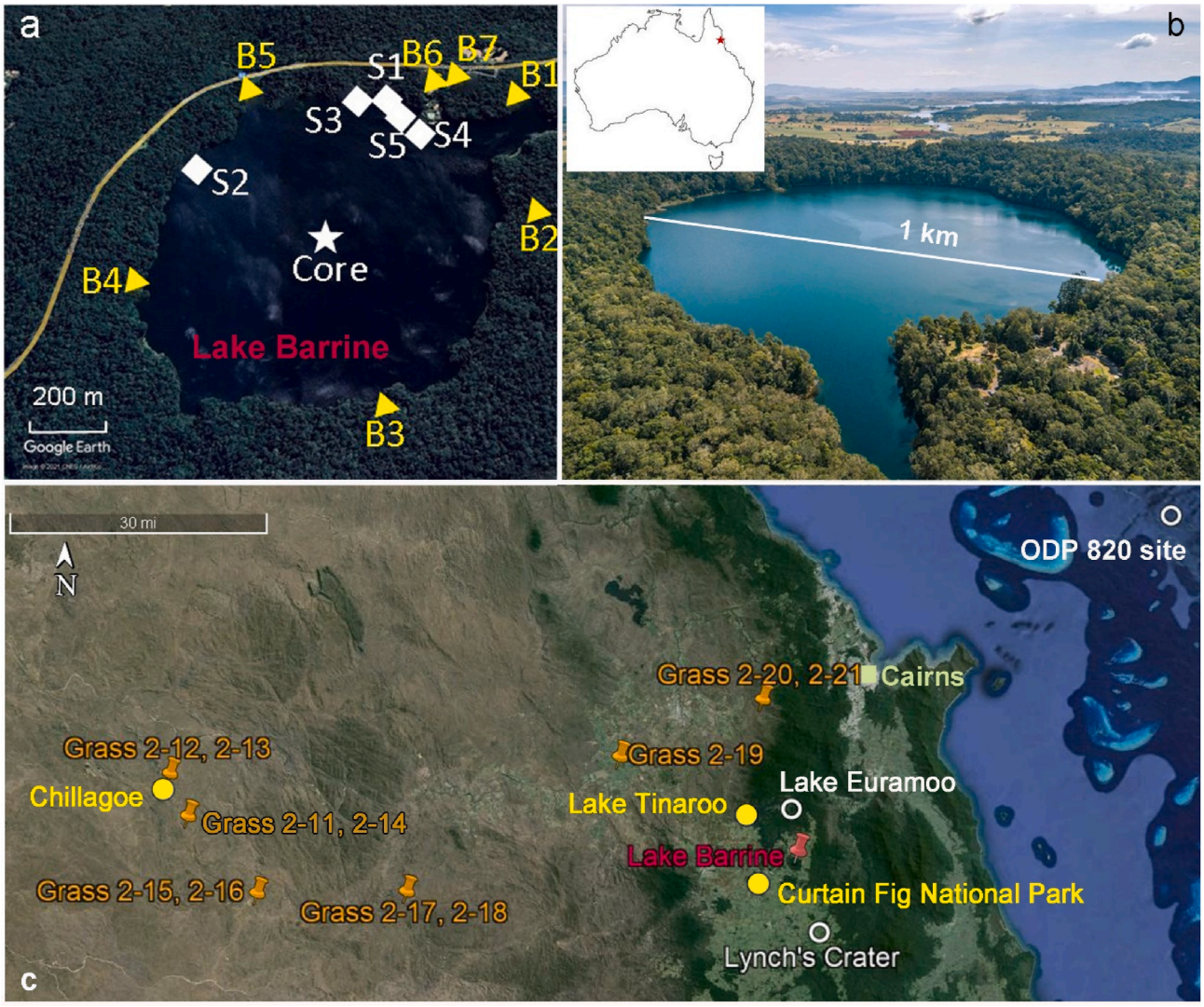

Fig. 1. Sampling sites and regional records used in this research. (a) The collection sites of the sediment core (white star), surface sediments (white diamonds, S1–S5), catchment soil and fallen leaves (yellow triangles, B1–B7). **(b)** The modern vegetation around Lake Barrine. **(c)** Sampling sites of the 18 fresh rainforest tree leaves (Curtain Fig National Park) and 11 grasses, as well as modern rainfall (Chillagoe) and inflow water **(**Lake Tinaroo). The red pin denotes the coring site at Lake Barrine while the white circles represent the locations of the regional records used for comparison with this study.

grasses are essentially all C_4 monocots while rainforest trees are all C_3 dicots. A combination of $\delta^{13}C$ and δ^2H analyses of *n*-alkanes from sediments provides a cross-check on climatic signals and can resolve ambiguities. Yet, this potential remains unexploited in this tropical region. Here, we combined the $\delta^{13}C$ and δ^2H values of the C_{31} *n*-alkane ($\delta^{13}C_{n\text{-}C31}$ and $\delta^2H_{n\text{-}C31}$) with pollen and temperature records in a 7-m-long sediment sequence from Lake Barrine spanning the period 18.3–1.7 cal ka BP (Li et al., 2022). We aim to (i) build a robust climatic record using multiple proxies to determine C_3 plant abundance in the catchment and monsoon intensity at Lake Barrine over the past 18.3 kyr, and (ii) form a broader view of paleo climatic change on the Atherton Tablelands in northeastern Australia.

2. Materials and methods

2.1. Research site, sample collection and chronology

Lake Barrine (17.25° S, 145.64° E, 726 m asl; Fig. 1) occupies a maar crater on the basaltic Atherton Tablelands, one of over 40 recognized volcanic eruption points (Timms, 1976) in north Queensland, tropical Australia. This lake is a small, flat-floored, freshwater maar lake with a surface area of 1.0 km^2, a diameter of 1.1 km and a total catchment area of 1.95 km^2 (Walker, 1999). The lake is surrounded by a crater rim of pyroclastics of low inclined outer slopes (15°, Jardine, 1925) and high inclined inner slopes (averaging ~30° and as high as 75°) (Timms, 1976). The maximum water depth of the lake is 68.3 m at present and varies ±0.5 m annually, constrained by an outflow to Toohey Creek (Timms, 1976) on the northeastern margin in the wettest months. The closed lake is recharged by direct precipitation, groundwater and surface runoff from the catchment basin, without any inlet rivers.

The mean annual air temperature at the site is around 21.2 ± 0.4 °C (1969–2020 CE, Walkamin research station, 2021a,b; Li et al., 2023). The mean annual precipitation is 1601 ± 481 mm (2000–2020 CE, Malanda Alert Station, 2021), over 80% of which is delivered during the wet season from December to March (Suppiah, 1992). The water table around Lake Barrine lied between 740 m and 680 m above sea level (a.s.l.) from 1991 to 2009 CE (Bore 92678 and 92710, 1991; Bore 148037 and 148111, 2009), similar to, or above the modern lake level (726 m a.s.l.). The mean $\delta^{18}O$ and δ^2H values of the water in Lake Barrine were 0.77‰ and −0.82‰, respectively, measured from the surface to the bottom of the lake water in December 2012 and July 2013 (Munksgaard, unpublished).

Modern vegetation growing on red ferrosol around Lake Barrine consists of ~3 km^2 remnant complex mesophyll vine forest (Fig. 1a and b; Tracey, 1982), with the original vegetation largely cleared for agriculture and pasture (Neldner et al., 2023). Complex mesophyll vine forest, in the Wet Tropics bioregion, represents optimally developed rainforest in Australia under the most favorable climate and soil conditions (Tracey, 1982). Distinct layers of vegetation develop, with the tallest trees and plank buttressing plants, such as robust woody lianas, vascular epiphytes, palms, and fleshy herbs with wide leaves. The closest sclerophyll woodland and savanna areas, with a canopy dominated by *Eucalyptus* spp., are ~28 km to the west of the lake (Chen, 1986).

In situ sediment cores were taken in October 2018, near the center of Lake Barrine in 68-m-deep water using a raft mounted Uwitec Piston corer with 6.5 cm diameter barrels (Fig. 1a). An almost 14-m-long sediment sequence was recovered, composed of five drives of ~3 m each. The sediment cores were transported to the lab and each core was cut into ~1-m sections to facilitate handling and minimize disturbance and kept vertically at −18 °C at the conclusion of the fieldwork. Each section was later split longitudinally into two halves – one half was archived while the other half was sampled. A combined 'master core' of 7.2 m in length was developed by correlating sections according to ages and excluding overlapping sections (see details in Li et al., 2022). Forty-eight subsamples were cut from the master core sediment sequence, with each subsample spanning 1–7 cm.

Additionally, surface lake sediments, fallen leaves and soils from the crater, fresh rainforest tree leaves and grasses were collected to study modern terrestrial plants and environment at Lake Barrine. Five surface lake sediment samples were collected from different locations within Lake Barrine and immediately frozen in the lab in November 2021 (Fig. 1a). Seven fallen leaf and seven soil samples were collected from around the crater in August 2021 to represent the terrestrial *n*-alkane source and to investigate the origin and the isotopic evolution of *n*-alkanes in the sediments (Fig. 1a).

Canopy leaves from 18 rainforest trees were collected in the mature rainforest in the Curtain Fig National Park, 8 km southwest of Lake Barrine in 2016 (Bauman et al., 2022). Six tree species were represented, with three individual trees sampled per species. The species were chosen on the basis that they made up 80% of the basal area in a 0.5 ha forest census plot in which all trees larger than 10 cm diameter at breast height had been identified and diameters measured over time (Metcalfe et al., 2014). Eleven samples of the most common grasses were collected on a transect from Cairns to Chillagoe, northern Queensland, 40–120 km away from Lake Barrine, in 2022 (Fig. 1c). These samples provide end-members of carbon and hydrogen isotope compositions from which to estimate the C_3 plant abundance and monsoon intensity in the past from the sedimentary record.

In addition, source waters for the rainforest tree leaves and grasses were collected to define the hydrogen net fractionation between source water and *n*-alkanes. Monthly water samples from catchments draining into Lake Tinaroo near Lake Barrine (Fig. 1c), 13 km north of the Curtain Fig Park, were collected from November 2018 to November 2020 and their isotope composition used as source water for the rainforest tree leaves. As Lake Tinaroo is only 6 km northwest to Lake Barrine, we used the δ^2H value of these waters to approximate the composition of precipitation at Lake Barrine. Accumulated weekly rainfall in Chillagoe (Fig. 1c) was collected on open ground from February 2015 to December 2022 using an International Atomic Energy Agency (IAEA)-designed Palmex rain collector which minimizes evaporation from the sample. These samples were used as the source water for the collected fresh grass samples.

Hydrogen isotope analyses of the inlet lake water and rainfall samples were conducted on a Picarro L2130i water isotope analyzer with its autosampler connected to a diffusion sampler device (Munksgaard et al., 2011). Measurements were scaled relative to the VSMOW using secondary water standards tied to the IAEA standards VSMOW2 and VSLAP2. Precision was typically ±0.5‰ for the δ^2H values of water (1σ standard deviation).

The chronology for the Lake Barrine sedimentary record was generated from ^{14}C analyses. Twenty-two radiocarbon measurements on selected samples were performed at the Radiocarbon Dating Laboratory at the University of Waikato in 2019 and 2020. The samples were made up of nine hand-picked organics, seven bulk sediments, three wood and three charcoal. These samples were washed in hot HCl, rinsed, and treated with multiple hot NaOH washes and then washed again with hot HCl, filtered, rinsed, and dried at the Waikato Radiocarbon Laboratory. An age-depth model was then developed based on the AMS ^{14}C ages and the 'master depth' using Bacon package (Blaauw and Christen, 2011) in R (R Core Team, 2020) and was then mapped onto the compound-specific isotope data series (for further details see Li et al., 2022, 2023). The ages of the catchment soils and surface lake sediments are unknown.

2.2. Lipid extraction, separation, and identification

Freeze dried sediment, soil and plant samples were ground into fine powder and 1–32 g dry mass of the powder was weighed for total lipid extraction. These powdered samples were ultrasonically agitated in dichloromethane: methanol = 9:1 (v:v; volume: volume) and were placed in a MARS 6 microwave digestion instrument for total lipid extraction at 100 °C for 21 min (ramp for 15 min and hold for 6 min).

The solid was removed from the total lipid extract (TLE) by rinsing each microwaved sample through a glass microfiber filter with a further ~20 mL DCM: methanol = 9:1 (v:v) three times. For all samples, the TLE was dried under a gentle stream of nitrogen. This total lipid extraction was completed in the Advanced Analytical Centre in James Cook University, Cairns, Australia.

n-Alkanes were then separated from the TLE using column chromatography. We prepared the columns by packing pre-ashed long pipettes with activated silica gel that was pre-washed using dichloromethane and methanol twice before drying at 50 °C. Hydrocarbons were eluted with *n*-hexane, although isoprenoids existed in the hydrocarbons in our case. We therefore separated *n*-alkanes from other hydrocarbons with double bonds by passing the hydrocarbons through $AgNO_3$-impregnated silica gel (10% by weight) chromatography in short columns using ~4 mL *n*-hexane. We then dried the *n*-alkanes using N_2 and transferred to GC vials for GC-MS and GC-IRMS measurements.

n-Alkanes were identified on gas chromatography-mass spectrometry (GC-MS) in the Lab of Isotopomics in Chemical Biology (ICB), Shaanxi University of Science and Technology, China and Advanced Analytical Center (AAC) in James Cook University, Australia. The GC-MS (ThermoScientific) in the ICB includes a Trace 1300 GC and an ISO single quadrupole mass selective detector system. The GC-MS (Shimadzu; GCMS-QP2010 SE) in the AAC includes an Agilent 7890A GC, Agilent 5975C quadrupole mass selective detector system and a flame ionization detector (FID). Compounds were separated on fused silica columns (Agilent J&W HP-5ms; 30 m × 0.25 mm, 25 μm film thickness in the ICB and Agilent J&W DB-5ms; 30 m × 0.25 mm, 25 mm film thickness in the AAC). The oven ramped from an initial temperature of 80 °C–150 °C at 15 °C/min, then to 250 °C at 30 °C/min and lastly to 310 °C (held 10 min) at 4 °C/min. Samples measured in the AAC were dissolved in *n*-hexane spiked with 25 μL 5α-androstane of 0.4 μg/μL as an internal standard before quantification. Compound peak areas were normalized to those of 5α-androstane and converted to concentration using response curves for an in-house mixture of C_{16}–C_{30} *n*-alkanes at concentrations ranging from 5 to 250 μg/mL. Recovery standards were not used and therefore we could not account for potential lipid loss during extraction and separation processes.

The fractional abundances of *n*-alkanes from C_{23} to C_{35} were calculated using Eq. (1)., where i denotes the absolute abundance of a given *n*-alkane, and C_{23}–C_{35} are the sum of absolute abundances of *n*-alkanes with 23–35 carbon atoms.

$$f(i) = i/\Sigma C_{23\text{-}35} \quad (1)$$

2.3. Carbon and hydrogen isotopic analyses

The carbon and hydrogen isotope compositions of individual *n*-alkane compounds were determined using gas chromatography isotope ratio mass spectrometry (GC-IRMS). These analyses were conducted in the Lab of Isotopomics in Chemical Biology, Shaanxi University of Science and Technology and Southern University of Science and Technology, China. A trace GC was coupled to an Isolink combustion/pyrolysis reactor (1000 °C for C and 1420 °C for H, respectively) and interfaced to a MAT-253 via a Conflo IV. The Trace GC was equipped with a non-polar capillary column HP-5ms and split/splitless injector was used for analyzing the samples. The purified *n*-alkane samples were injected into the GC oven in splitless mode with an inlet temperature of 300 °C and helium as carrier gas. The GC oven temperature ramp was the same as that for GC-MS.

Before measuring hydrogen isotope compositions, an H_3^+ factor correction was determined and was <11 ppm/nA, indicating a contribution of <0.11% H_3^+ to HD^+. During the C and H isotope measurements, the precision of the isotope analyses was routinely checked after every six sample injections by injecting one/two A7 standard of C_{16}–C_{30} *n*-alkanes with known $\delta^{13}C$ and δ^2H values (A. Schimmelmann, Indiana University). Linearity and drift corrections were applied to both C and H isotope measurements to correct instrument offset and only values with voltages above 300 mV and 500 mV respectively, were used for these two isotope measurements. The $\delta^{13}C$ values of *n*-alkanes were normalized to the Vienna Peedee Belemnite (VPDB) while the δ^2H values were normalized to the Vienna Standard Mean Ocean Water (VSMOW) scales. The analytical precisions (1σ) for carbon and hydrogen isotope compositions of standards were better than 0.4‰ and 5‰, respectively.

We corrected the measured carbon isotope compositions of modern *n*-alkane samples to account for changes in atmospheric ^{13}C due to fossil fuel burning. We added 1.6‰ to the $\delta^{13}C$ values of *n*-alkanes from modern samples, including fresh grasses, fresh rainforest tree leaves, and fallen leaves, because the average $\delta^{13}C$ value of the present atmosphere is −8‰ while that of the pre-industrial atmosphere was −6.4‰ (McCarroll and Loader, 2004). We did not correct the $\delta^{13}C$ values of *n*-alkanes from the surface sediments as we assume the lake sediments are dominated by pre-industrial *n*-alkanes. We added 0.8‰ to the $\delta^{13}C$ values of *n*-alkanes from the catchment soils because they could have an intermediate age and contain a mix of pre-industrial and post-industrial *n*-alkanes.

We also corrected the measured δ^2H values of *n*-alkanes from the sediments to offset changes in water isotope composition due to changes in ice volume since the Last Glacial Maximum (LGM). Changes in ice volume on glacial-interglacial timescales impact the δ^2H values of precipitation due to changes in the isotope composition of seawater. A 1‰ increase in the $\delta^{18}O$ values of seawater ($\delta^{18}O_{sw}$) during the LGM has been suggested (Schrag et al., 1996; Shackleton, 2000) and a time series of $\delta^{18}O_{sw}$ values was developed in the tropical western Pacific (Scroxton et al., 2022) based on the modeled global $\delta^{18}O_{sw}$ values (Lisiecki and Raymo, 2005). We therefore converted the $\delta^{18}O_{sw}$ values into δ^2H values of seawater (δ^2H_{sw}) using the Global Meteoric Water Line (Craig, 1961) assuming a deuterium excess of zero (Vimeux et al., 2001). We then subtracted the δ^2H_{sw} values from the measured δ^2H values of *n*-alkanes from the surface and downcore sediments in this study.

2.4. Estimation of the fraction of C_3 plants and the δ^2H values of precipitation

Despite the influence from precipitation and temperature, sedimentary $\delta^{13}C$ values of the C_{31} *n*-alkane ($\delta^{13}C_{n\text{-}C31}$) mainly reflect changes in the proportions of C_3 and C_4 plants deposited in the sediments (O'Leary, 1981; Diefendorf and Freimuth, 2017). Therefore, we applied a linear binary mixing model (vegetation composition model; Eq. (2)) to the $\delta^{13}C_{n\text{-}C31}$ values of the lake sediments to estimate the fractions of C_3 and C_4 plants in the catchment of Lake Barrine since 18.3 cal ka BP. On the other hand, as photosynthetic pathways are not the only factor that influences the $\delta^{13}C$ values of plants, we acknowledge that this model is an estimation that may not capture all sources of uncertainty. The two end members in the binary mixing model were the corrected average $\delta^{13}C_{n\text{-}C31}$ values of the 11 grasses (−19.9 ± 2.5‰; with a range of −24.9‰ to −17.9‰) and 18 rainforest tree leaves (−37.3 ± 1.5‰; ranging from −39.6‰ to −35.4‰), respectively.

$$\delta^{13}C_{n\text{-}C31\_sed} = fC_3 * \delta^{13}C_{n\text{-}C31\_C3} + (1 - fC_3) * \delta^{13}C_{n\text{-}C31\_C4} \quad (2)$$

where fC_3 and (1 - fC_3) are the fractions of C_3 and C_4 plants, respectively. $\delta^{13}C_{n\text{-}C31\_sed}$, $\delta^{13}C_{n\text{-}C31\_C3}$ and $\delta^{13}C_{n\text{-}C31\_C4}$ are the average $\delta^{13}C$ values of C_{31} *n*-alkane from sediment in Lake Barrine, 18 rainforest tree leaves, and 11 grasses in this study, respectively.

Similarly, we applied a vegetation correction (Eq. (3); 4; 5) to the δ^2H values of precipitation reconstructed from the lake sediments using another linear binary mixing model (vegetation-corrected precipitation model). This model was based on the fractions of C_3 and C_4 plants in the sediment reconstructed from the vegetation composition model, and the hydrogen isotope fractionation between precipitation and C_{31} *n*-alkane

($\varepsilon_{C31\text{-}P}$; Eq. (3)) in C_3 and C_4 plants. This method has been successfully employed in other tropical studies (Feakins, 2013; Shanahan et al., 2015; Konecky et al., 2016).

$$\varepsilon_{C31\text{-}P} = [(\delta^2H_{n\text{-}C31} + 1000)/(\delta^2H_P + 1000) - 1] * 1000\ (‰) \quad 3$$

where $\varepsilon_{C31\text{-}P}$ refers to the net fractionations between the δ^2H values of precipitation and C_{31} *n*-alkanes. $\delta^2H_{n\text{-}C31}$ denotes the hydrogen isotope compositions (δ^2H) of C_{31} *n*-alkane while δ^2H_P refers to the δ^2H values of local precipitation. All epsilon values herein are interpreted based on their absolute values (e.g., larger ε_{app} means that the absolute ε_{app} value is greater).

$$\varepsilon_{C31\text{-}P\_veg} = fC_3 * \varepsilon_{C31\text{-}P\_C3} + (1 - fC_3) * \varepsilon_{C31\text{-}P\_C4} \quad 4$$

$$\delta^2H_{P\text{-}R} = [(\delta^2H_{n\text{-}C31\_sed} + 1000) / (\varepsilon_{C31\text{-}P\_veg} / 1000 + 1)] - 1000 \quad 5$$

where fC_3 and (1- fC_3) denote the fractions of C_3 and C_4 plants, respectively. $\varepsilon_{C31\text{-}P\_C3}$ and $\varepsilon_{C31\text{-}P\_C4}$ refer to the average net fractionations between precipitation and C_{31} *n*-alkane ($\varepsilon_{C31\text{-}P}$) of the 18 rainforest tree leaves and 11 grasses in this study, respectively. $\varepsilon_{C31\text{-}P\_veg}$ is vegetation-corrected $\varepsilon_{C31\text{-}P}$. $\delta^2H_{P\text{-}R}$ is the reconstructed δ^2H values of precipitation while $\delta^2H_{n\text{-}C31\_sed}$ is the measured $\delta^2H_{n\text{-}C31}$ values of the lake sediments.

The two end members in the vegetation-corrected precipitation model were the average $\varepsilon_{C31\text{-}P}$ values of the 11 grasses ($\varepsilon_{C31\text{-}P\_C4}$; −181.5 ± 15.5 ‰) and 18 rainforest tree leaves ($\varepsilon_{C31\text{-}P\_C3}$; −96.1 ± 15.2 ‰) (Fig. 3c). The $\varepsilon_{C31\text{-}P}$ values were calculated based on Eq. (3), using the measured $\delta^2H_{n\text{-}C31}$ values of the grass and rainforest tree leaf samples and δ^2H values of precipitation (δ^2H_P). We used the average δ^2H values of rainfall in Chillagoe (−28.2‰; Table S1) and inlet water of Lake Tinaroo (−34.0‰; Table S2) as the δ^2H values of source waters of the grasses and rainforest tree leaves, respectively. Based on Eq. (4), the estimated fraction of C_3 plants, and the two end members ($\varepsilon_{C31\text{-}P\_C3}$ and $\varepsilon_{C31\text{-}P\_C4}$), we then calculated the vegetation-corrected $\varepsilon_{C31\text{-}P}$ values ($\varepsilon_{C31\text{-}P\_veg}$) for the lake sediments, soils, and fallen leaf mixtures. Using Eq. (5), we reconstructed the δ^2H values of precipitation ($\delta^2H_{P\text{-}R}$) using the ice volume corrected $\delta^2H_{n\text{-}C31}$ values and estimated $\varepsilon_{C31\text{-}P\_veg}$ values of the sediments in Lake Barrine over the past 18.3 kyr (Eq. (5)).

Over 80% of total precipitation at Lake Barrine occurs from December to March when the Indonesian-Australian summer monsoon (IASM) dominates local rainfall (Suppiah, 1992). Additionally, modern hydroclimate studies have shown that the IASM and cyclones bring precipitation with lower δ^2H values to tropical northern Australia compared to other winds, including the southeast trade winds (Munksgaard et al., 2012; Zwart et al., 2018). Therefore, rainfall amount is negatively correlated to the δ^2H values of precipitation (δ^2H_P) brought by the IASM but not by other winds in this region (Zwart, 2021). For example, the southeast trade winds bring precipitation of high δ^2H values (up to 0‰) (Munksgaard et al., 2012), which induces no amount effect (Zwart et al., 2018). We therefore interpreted the $\delta^2H_{P\text{-}R}$ values as a measure of the IASM intensity – whereby lower $\delta^2H_{P\text{-}R}$ values indicate stronger IASMs generating higher rainfall and vice versa.

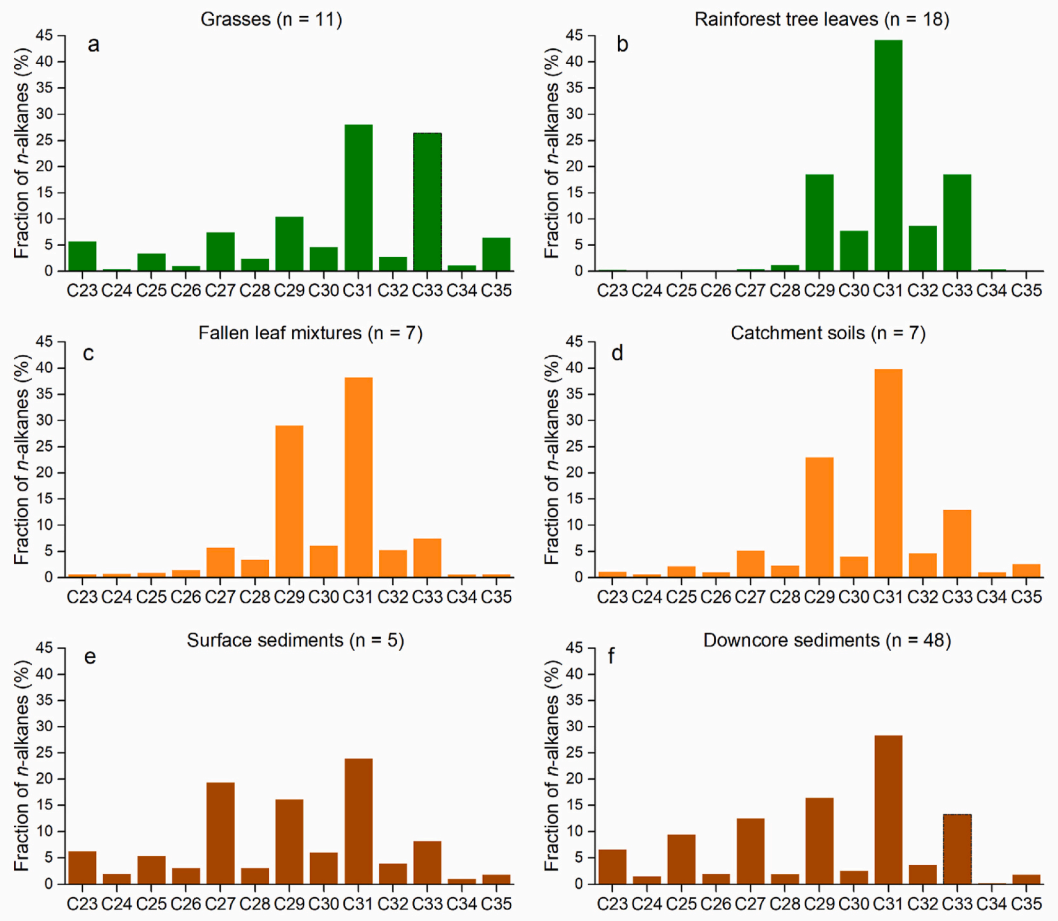

Fig. 2. The average fractional distributions of C_{23}–C_{35} *n*-alkanes. (a) the modern grasses; **(b)** rainforest tree leaves; **(c)** the fallen leaf mixtures and **(d)** catchment soils around Lake Barrine; **(e)** the surface and **(f)** downcore sediments in Lake Barrine. The color scheme from green to orange and brown indicates *n*-alkanes from fresh plants to sedimentary archives.

3. Results

3.1. The fractional abundance, $\delta^{13}C$ and $\delta^{2}H$ values of long-chain *n*-alkanes from modern samples

For fractional abundance, the *n*-C_{31} dominated in all modern plant and soil samples, followed by *n*-C_{29} or *n*-C_{33} (Fig. 2). The *n*-C_{31} composed 42%, 38%, 40%, and 28% of the total *n*-alkanes from the 18 rainforest tree leaves, seven fallen leaf mixtures in the catchment, seven catchment soils, and 11 grasses, respectively. The *n*-C_{29} was the second most abundant in the rainforest tree leaves, fallen leaf mixtures and catchment soils (Fig. 2b-d), while in grass samples, the *n*-C_{33} (26%) was the second most abundant (Fig. 2a). The *n*-alkanes of long odd chains (C_{27}, C_{29}, C_{31}, C_{33}) made up the highest proportions (>72%) of the total *n*-alkanes whereas mid-chain (C_{21}–C_{26}) *n*-alkanes constitute less than 11% in all the modern samples.

In the modern plants, the $\delta^{13}C_{n\text{-}C29}$, $\delta^{13}C_{n\text{-}C31}$, $\delta^{13}C_{n\text{-}C33}$ values of each sample are similar, with subtle differences (Fig. 3a). The average

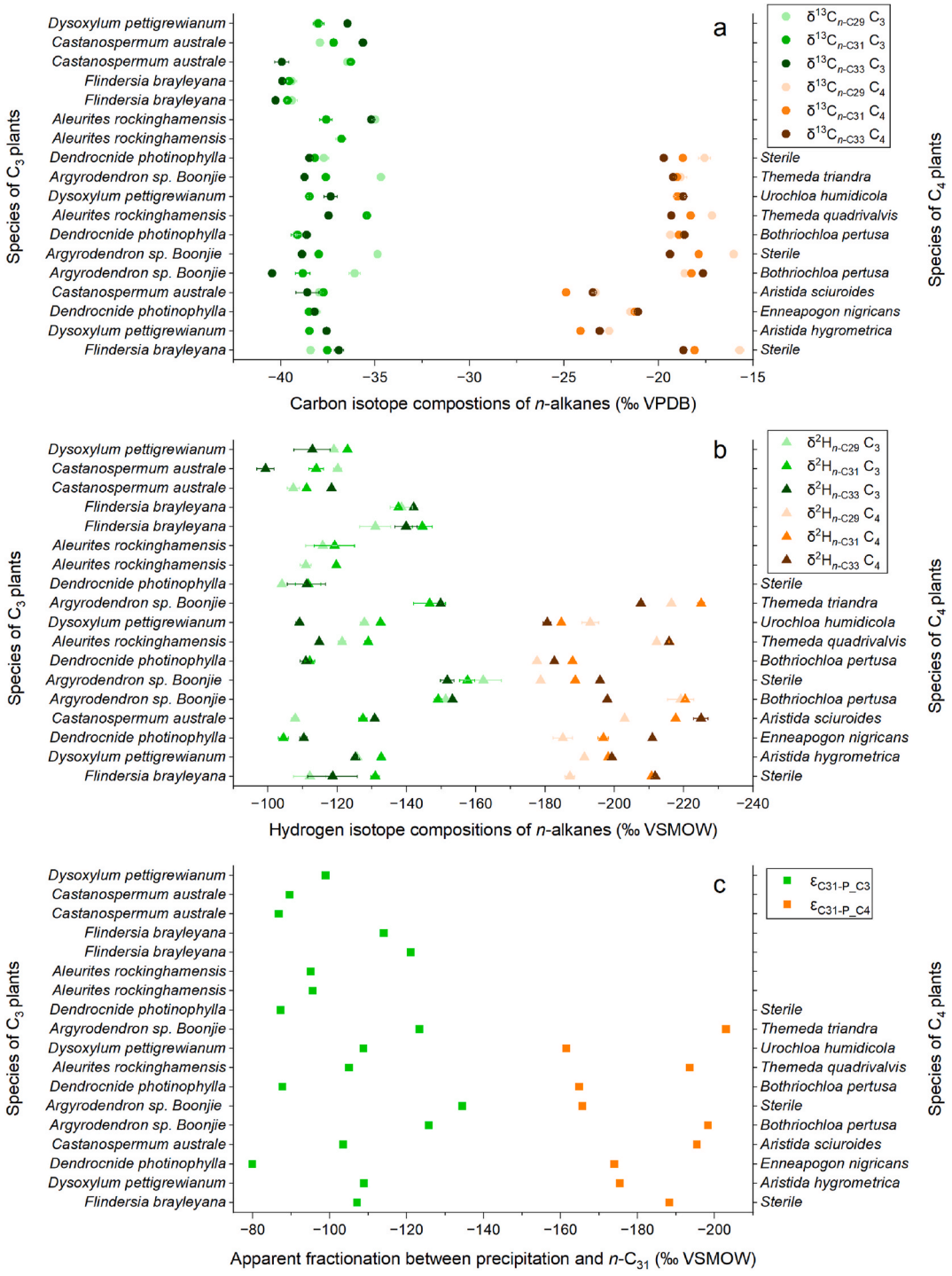

Fig. 3. The average $\delta^{13}C$ (a) and $\delta^{2}H$ values (b) of *n*-C_{29}, *n*-C_{31} and *n*-C_{33} and net fractionation between precipitation and *n*-C_{31} (c) in modern grasses and rainforest tree leaves. In **a**, the $\delta^{13}C_{n\text{-}C31}$ values were corrected for fossil fuel burning (see Methods). Green and orange symbols denote C_3 rainforest tree leaves and grasses, respectively. *Argyrodendron* sp. *Boonjie* in C_3 plants is *Argyrodendron* sp. *Boonjie* (*B.P.Hyland RFK 2139*) and the bottom two Sterile in C_4 plants are possibly *Heteropogon contortus*.

$\delta^{13}C_{n\text{-}C29}$ values were slightly higher than the average $\delta^{13}C_{n\text{-}C31}$ values of grass and rainforest tree leaf samples (−19.0 ± 2.5‰ and −19.9 ± 2.5‰, −37.5 ± 1.5‰ and −37.9 ± 1.1‰, respectively). By comparison, C_{33} and C_{31} *n*-alkanes from the modern plant samples had nearly the same $\delta^{13}C$ values (−19.9 ± 1.9‰ and −19.9 ± 2.5‰ for grasses, −38.2 ± 1.5‰ and −37.9 ± 1.1‰ for rainforest tree leaves, respectively). The average $\delta^{13}C_{n\text{-}C31}$ values of the seven rainforest fallen leaf mixtures and seven soil samples around Lake Barrine were similar, −37.5 ± 0.98‰ and −37.1 ± 0.59‰, respectively. However, the $\delta^{13}C_{n\text{-}C31}$ values of modern rainforest (−37.9 ± 1.1‰), fallen leaf mixtures and soil samples were close but presenting a slight increasing trend.

In terms of hydrogen isotope composition of the modern plant samples, the $\delta^{2}H_{n\text{-}C29}$ values were similar to, but slightly higher than, the corresponding $\delta^{2}H_{n\text{-}C31}$ values (Fig. 3b). The average $\delta^{2}H_{n\text{-}C31}$ value of the 18 rainforest tree leaves was −127.9 ± 15‰ while that of the 11 grasses was −204.6 ± 15‰, on average 77‰ lower than that of rainforest tree leaves. The average $\delta^{2}H_{n\text{-}C29}$ value of the rainforest tree leaves was −123.6 ± 17‰ compared to −196.4 ± 15‰ of the grasses, 73‰ lower than that of rainforest tree leaves. The seven soil samples and seven fallen leaf mixtures around Lake Barrine have similar average $\delta^{2}H_{n\text{-}C31}$ values, −146.1 ± 9.8‰ and −145.4 ± 12.0‰, respectively, −19‰ lower than that of the fresh rainforest tree leaf samples. The average net fractionation between *n*-C_{31} and precipitation ($\varepsilon_{C31\text{-}P}$) in the 11 grasses ($\varepsilon_{C31\text{-}P\_C4}$) was −181.5 ± 15.5 ‰ ranging from −202.5‰ to −161.0‰ while that in the 18 rainforest tree leaves ($\varepsilon_{C31\text{-}P\_C3}$) was −96.1 ± 15.2 ‰ with a range of −127.9‰ to −72.9‰ (Fig. 3c; Table S3).

3.2. The fractional abundance, $\delta^{13}C$ and $\delta^{2}H$ values of long-chain *n*-alkanes from the lake sediments

The *n*-C_{31} also dominates in the sediments of Lake Barrine (Fig. 2e; 2f). The *n*-C_{31} alkane constitutes 22% and 28% of the total *n*-alkanes from surface and downcore lake sediments respectively, generally lower than the modern samples. The *n*-C_{29} was the second most abundant in the downcore sediments. In surface sediment samples, however, the *n*-C_{27} (18%) had the second highest proportion, while none of the modern terrestrial samples contained such a high fraction of *n*-C_{27}. Long odd chain *n*-alkanes, *n*-C_{27}, *n*-C_{29}, *n*-C_{31} and *n*-C_{33} formed the highest proportions (>62%) of total *n*-alkanes in the sediment samples whereas mid-chain (C_{21}–C_{26}) *n*-alkanes were 19%, slightly higher than those in the modern samples.

In the surface sediments of Lake Barrine, the average $\delta^{13}C_{n\text{-}C29}$ values (−34.0 ± 1.2‰) are much higher than $\delta^{13}C_{n\text{-}C31}$ (−36.7 ± 0.4‰) and $\delta^{13}C_{n\text{-}C33}$ values (−36.9 ± 0.5‰) compared to modern terrestrial plants. In the sedimentary sequence, the $\delta^{13}C$ values of *n*-C_{29}, *n*-C_{31} and *n*-C_{33} ($\delta^{13}C_{n\text{-}C31}$, $\delta^{13}C_{n\text{-}C33}$) track each other closely over the past 18.3 kyr (Fig. 4a; Table S4). The $\delta^{13}C_{n\text{-}C29}$ values of the sediments in Lake Barrine were higher than the $\delta^{13}C_{n\text{-}C31}$ values after 6.9 cal ka BP but lower or close to $\delta^{13}C_{n\text{-}C31}$ values before that. However, the $\delta^{13}C_{n\text{-}C33}$ values were virtually the same as the $\delta^{13}C_{n\text{-}C31}$ values during two periods, 6.9 cal ka BP–the present and 18.3–14.9 cal ka BP, but were usually higher than $\delta^{13}C_{n\text{-}C31}$ values by ~2‰ from 14.6 to 6.9 cal ka BP.

As the trends for the different *n*-alkanes are similar, here we only describe the $\delta^{13}C$ values of the most abundant component, *n*-C_{31}, in the lake sediments (Table S4). The $\delta^{13}C$ values of *n*-C_{31} ($\delta^{13}C_{n\text{-}C31}$) from the lake sediments were the highest (−23.0 ± 0.1‰) at 17.5 cal ka BP and decreased generally thereafter. The only continuous increase (by 4‰) in the $\delta^{13}C_{n\text{-}C31}$ values of the sediments occurred from 12.8 to 11.2 cal ka BP. The $\delta^{13}C_{n\text{-}C31}$ values reached the lowest value (−35.5 ± 0.0‰) at 6.1 cal ka BP and increased slightly thereafter to 1.7 cal ka BP (−34.8 ± 0.1‰), ~2‰ higher than the average $\delta^{13}C_{n\text{-}C31}$ value of the surface sediments (−36.7 ± 0.4‰). The average $\delta^{13}C_{n\text{-}C31}$ value of the modern surface sediments is slightly higher than that of the seven catchment soil samples (−37.1 ± 0.6‰) around Lake Barrine (Table S4).

Concerning hydrogen isotope composition, we mainly compared the $\delta^{2}H$ values of C_{29} and C_{31} *n*-alkanes ($\delta^{2}H_{n\text{-}C29}$ and $\delta^{2}H_{n\text{-}C31}$) because small peak sizes could have affected some of the $\delta^{2}H$ values of C_{33} *n*-alkane ($\delta^{2}H_{n\text{-}C33}$) even after correction. In the sedimentary record from Lake Barrine, the $\delta^{2}H_{n\text{-}C29}$ and $\delta^{2}H_{n\text{-}C31}$ values displayed similar decrease-then-increase trends over the past 18 kyr, with the inflection occurring at 6.1 cal ka BP (Fig. 4b; Table S4). The $\delta^{2}H_{n\text{-}C31}$ and $\delta^{2}H_{n\text{-}C29}$ values of the lake sediments were similar after 6.9 cal ka BP. However, the $\delta^{2}H_{n\text{-}C31}$ values were lower than the $\delta^{2}H_{n\text{-}C29}$ values during periods 12.8–ca. 6.9 cal ka BP and 18.3–ca. 15.7 cal ka BP, and higher than the $\delta^{2}H_{n\text{-}C29}$ values from 15.7 to 13.4 cal ka BP.

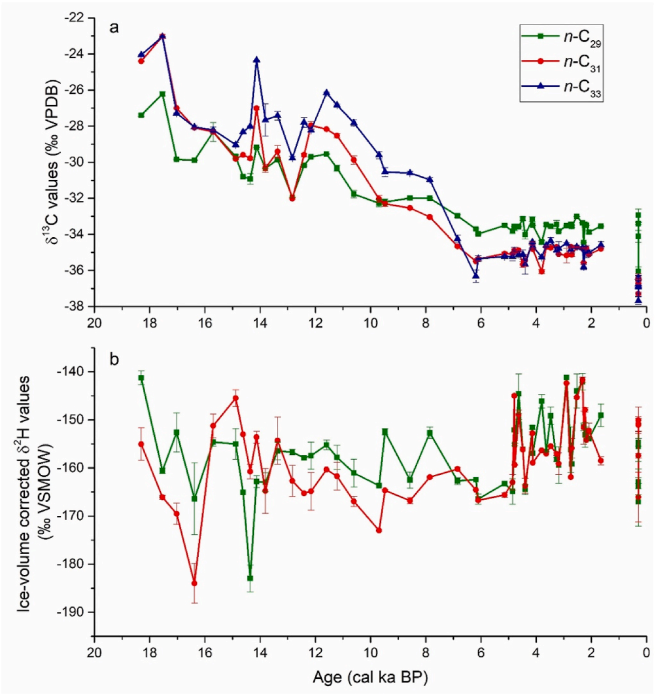

Fig. 4. The average $\delta^{13}C$ values of *n*-C_{29}, *n*-C_{31} and *n*-C_{33} (a) and average $\delta^{2}H$ values of *n*-C_{29} and *n*-C_{31} (b) from the downcore and surface sediments in Lake Barrine since 18.3 cal ka BP. The blue, red and dark gray lines denote *n*-C_{29}, *n*-C_{31} and *n*-C_{33}, respectively, and the corresponding shades are measurement uncertainties (standard deviation).

Likewise, we only describe trends in the $\delta^{2}H_{n\text{-}C31}$ values of the lake sediments over the full record (Fig. 4b; Table S4). From 18.3 to 16.4 cal ka BP, the ice-volume corrected $\delta^{2}H_{n\text{-}C31}$ values of the lake sediments decreased from −155.1 ± 3.4‰ to −184.0 ± 4.1‰, the lowest point of the record. From 16.4 to 14.9 cal ka BP, this value increased rapidly and reached the highest (−145.5 ± 1.7‰) values in the record. From 14.9 to 9.7 cal ka BP, the $\delta^{2}H_{n\text{-}C31}$ value decreased consistently to −173.0‰. From 9.7 to 1.7 cal ka BP, this value increased again to −158.5 ± 0.8‰, with multiple individual further peaks to around −140‰ in the late Holocene. The average $\delta^{2}H_{n\text{-}C31}$ value of the modern surface lake sediments (−155.1 ± 6.8‰) is close to that of the sediment at 1.7 cal ka BP (−158.5 ± 0.8‰).

3.3. The C_3 plant fraction and $\delta^{2}H$ estimates of precipitation ($\delta^{2}H_{P\text{-}R}$) at Lake Barrine

According to the vegetation composition model (Eq. (2)), the fraction of C_3 plants in the catchment of Lake Barrine increased overall from 17.5 cal ka BP to the present from 18% to 93% (Fig. 5a; Table S4). C_3 plants were slightly more abundant at 18.3 cal ka BP (25%) compared to those at 17.5 cal ka BP (18%), although this observation is based on a single sample. From 17.5 to 12.8 cal ka BP, the fraction of C_3 plants rose to 67% but then decreased to 45% from 12.8 to 12.1 cal ka BP. After a general increase thereafter, C_3 plants reached 86% at 6.1 cal ka BP and

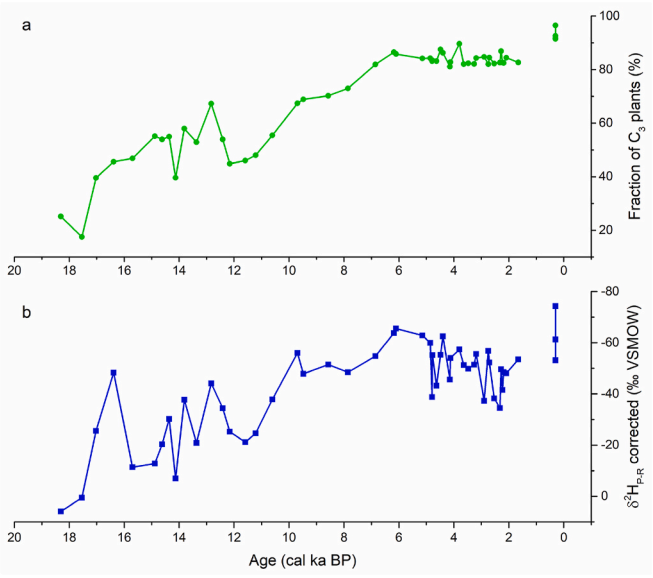

Fig. 5. The reconstructed fraction of C_3 plants in the catchment (a) and the δ^2H values of precipitation ($\delta^2H_{P\text{-}R}$) over Lake Barrine (b) over the period of 18.3–1.7 cal ka BP.

then remained stable to 1.7 cal ka BP. C_3 plants contributed ~93% to the modern sediment according to the average $\delta^{13}C_{n\text{-}C31}$ value of the five surface sediment samples, close to the observed modern C_3 plant percentage (effectively 100%). As a test, the reconstructed modern fraction of C_3 plants using the $\delta^{13}C_{n\text{-}C31}$ values of the seven catchment soils and the seven fallen leaf mixtures around Lake Barrine are 95% and 98%, respectively.

According to the vegetation-corrected precipitation model (Eq. (3); 4; 5), the reconstructed δ^2H values of precipitation ($\delta^2H_{P\text{-}R}$) over Lake Barrine generally decreased from 18.3 cal ka BP to the present, with the highest and lowest values occurring at 18.3 and 6.1 cal ka BP, respectively (Fig. 5b; Table S4). From 18.3 to 12.8 cal ka BP, the $\delta^2H_{P\text{-}R}$ value decreased from +5.9‰ to −44.1‰, with a particular rapid decrease to −48.3‰ at 16.4 cal ka BP. From 14.9 to 12.8 cal ka BP, this value decreased from −12.8‰ to −44.1‰, followed by an increase to −21.1‰ from 12.8 to 11.6 cal ka BP. From 11.6 to 6.1 cal ka BP, the $\delta^2H_{P\text{-}R}$ value generally decreased and reached the lowest value (−65.5‰) at 6.1 cal ka BP in the mid-Holocene. The $\delta^2H_{P\text{-}R}$ value thereafter fluctuated erratically and overall increased to −53.5‰ from 6.1 to 1.7 cal ka BP. The modern average $\delta^2H_{P\text{-}R}$ value (−59.0 ± 9.2‰) from the five surface sediments is close to the estimate at 1.7 cal ka BP. The modern $\delta^2H_{P\text{-}R}$ estimates using surface sediments is lower than those using the seven catchment soils (−51.2 ± 11.9‰) and seven fallen leaf mixtures (−52.4 ± 18.6‰) around Lake Barrine, and lower than the measured modern δ^2H values of precipitation (−34.0‰; Table S2).

4. Discussion

All the sediment, soil and plant samples we investigated in this study contained C_{23}–C_{35} *n*-alkanes, but we interpret the vegetation and precipitation changes in the Barrine record based mainly on *n*-C_{31}. The reasons are as follows: (1) Long-chain (C_{29}, C_{31}, C_{33} and C_{35}) *n*-alkanes are known to derive mainly from terrestrial plants (Zhao et al., 2021). (2) The *n*-C_{31} is the most abundant in sediments in Lake Barrine (Fig. 2). (3) The $\delta^{13}C$ values of *n*-C_{29}, *n*-C_{31} and *n*-C_{33} from the sediments in Lake Barrine displayed very similar trends over time, which indicates they are from similar sources. (4) Compared to *n*-C_{29}, the *n*-C_{31} is unlikely to have a significant aquatic component (Aichner et al., 2010; Zhao et al., 2021). For example, according to Zhao et al. (2021), aquatic flora in tropical lakes contain minor (3.2%) *n*-C_{29} but only trace *n*-C_{31} (0.6%). (5) Trees and grasses have more equivalent proportions of *n*-C_{31} compared to *n*-C_{33} (Fig. 2a; b).

4.1. Correlations among the n-alkanes from modern plants, soils and surface sediments

The average fractional abundances of *n*-C_{23} – *n*-C_{35} indicated that *n*-C_{31} dominates in all modern plant, soil and surface sediment samples, followed by *n*-C_{29}, *n*-C_{33} or *n*-C_{27} (Fig. 2). The lower fractional abundances of *n*-C_{28}, *n*-C_{29}, *n*-C_{30} and higher *n*-C_{33} in fallen leaves compared to soil samples may suggest longer-chain *n*-alkanes tend to preserve more easily due to their higher stability. The second most abundant component, *n*-C_{27}, in surface sediments may suggest an aquatic plant and/or algal contribution as all the terrestrial plant samples have lower percentages of *n*-C_{27}. In the fresh plant samples, the $\delta^{13}C_{n\text{-}C29}$ values are similar to, but slightly higher than, the $\delta^{13}C_{n\text{-}C31}$ and $\delta^{13}C_{n\text{-}C33}$ values (by 0.9‰ in the grasses and by 0.4‰ in the rainforest leaves), which may result from lower $\delta^{13}C$ values in the carbon atoms added from acetyl-CoA during biosynthesis (Zhou et al., 2010).

In the surface sediments, however, the $\delta^{13}C_{n\text{-}C29}$ values (−34.0 ± 1.2‰) are 2.7‰ higher compared to the $\delta^{13}C_{n\text{-}C31}$ (−36.7 ± 0.4‰) and $\delta^{13}C_{n\text{-}C33}$ values (−36.9 ± 0.5‰), suggesting a *n*-C_{29} contribution from aquatic plants. Moreover, a slight increasing trend exists in the corrected $\delta^{13}C_{n\text{-}C31}$ (same for $\delta^{13}C_{n\text{-}C29}$ and $\delta^{13}C_{n\text{-}C33}$) values from fresh rainforest leaves (−37.9 ± 1.1‰), to fallen leaves (−37.5 ± 1.0‰), soils (−37.1 ± 0.6‰) and surface sediments (Fig. 6a), which possibly indicates a small degree of ^{13}C enrichment over time. This enrichment has been noticed in the $\delta^{13}C$ values of *n*-alkanes from plants and soils and is suggested to be due to degradation (Nguyen Tu et al., 2004; Chikaraishi and Naraoka, 2006; Brittingham et al., 2017).

In the rainforest and grass leaf samples, the slightly higher $\delta^2H_{n\text{-}C29}$ values (−124.2 ± 16.3‰ and 196.4 ± 15.0‰, respectively) compared to the $\delta^2H_{n\text{-}C31}$ values (−126.8 ± 14.7‰ and −204.6 ± 15.0‰) and $\delta^2H_{n\text{-}C33}$ values (−127.6 ± 18‰; −202.7 ± 14.0‰) are possibly due to the lower δ^2H values of the hydrogen atoms added from NADPH during biosynthesis (Zhou et al., 2010). Interestingly, the $\delta^2H_{n\text{-}C31}$ (same for $\delta^2H_{n\text{-}C29}$ and $\delta^2H_{n\text{-}C33}$) values exhibit an obvious decreasing trend from the fresh rainforest leaves (−126.8 ± 14.7‰), to the rainforest fallen leaf mixture (−145.5 ± 12.0‰), catchment soils (−146.1 ± 9.8‰), and surface sediments (−155.1 ± 6.8‰) (Fig. 6b). A similar amount of deuterium depletion (over −15‰) is observed in other research and suggested to be a result of a build-up of microbial *n*-alkanes during decomposition and/or diagenesis (Zech et al., 2011).

4.2. Paleo vegetation and precipitation change at Lake Barrine

The reconstructed fraction of C_3 plants in the catchment is potentially close to the true fraction of C_3 plants over time, as the estimated modern percentage of C_3 vegetation is 93% (Fig. 5a; Table S4) while the observed value is ~100%. The C_3 plant percentage (25–18%) during 18.3–17.5 cal ka BP suggests that the catchment around Lake Barrine was probably mostly covered by grassy open savanna. C_3 plants increased from 18% to 67% during 17.5–12.8 cal ka BP, indicating a progression to a higher woody canopy cover. After a brief decrease during 12.8–11.6 cal ka BP (the Younger Dryas), the woody plants continuously developed to 86% at 6.1 cal ka BP, potentially forming the rainforest canopy since then.

The average modern δ^2H estimate of precipitation (−59.0 ± 9.2‰) using surface sediments is −25‰ lower than the measured values (−34.0‰). This is probably because ^2H is depleted in *n*-alkanes during the sedimentary process of fresh rainforest leaves into soils, in which −19‰ depletion occurred in $\delta^2H_{n\text{-}C31}$ values (see Section 4.1). This phenomenon suggests that the soils below modern plants may be better end members for reconstructing the δ^2H values of precipitation.

The $\delta^2H_{P\text{-}R}$ values over Lake Barrine decreased from 18.3 cal ka BP to the present (Fig. 5b; Table S4), indicating a general trend to wetter,

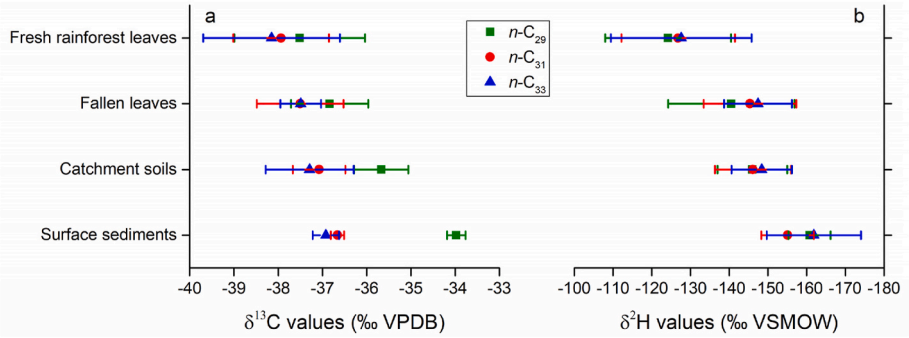

Fig. 6. The trends of ^{13}C enrichment and ^{2}H depletion in n-C_{29}, n-C_{31} and n-C_{33} in fresh rainforest leaves, fallen leaves, soils and surface sediments.

more monsoonal conditions. The highest and lowest $\delta^2H_{P\text{-}R}$ values occurred at 18.3 cal ka BP and 6.1 cal ka BP, respectively, suggesting the driest and wettest periods at Lake Barrine over the past 18,300 years occurred at these times. From 18.3 to 12.8 cal ka BP, the $\delta^2H_{P\text{-}R}$ value decreased from +5.9‰ to −44.1‰, with a particular rapid decrease to −48.3‰ at 16.4 cal ka BP, suggesting brief wet conditions at that time. From 14.9 to 12.8 cal ka BP, $\delta^2H_{P\text{-}R}$ value decreased from −12.8‰ to −44.1‰, which may also suggest wetter conditions pertained during the

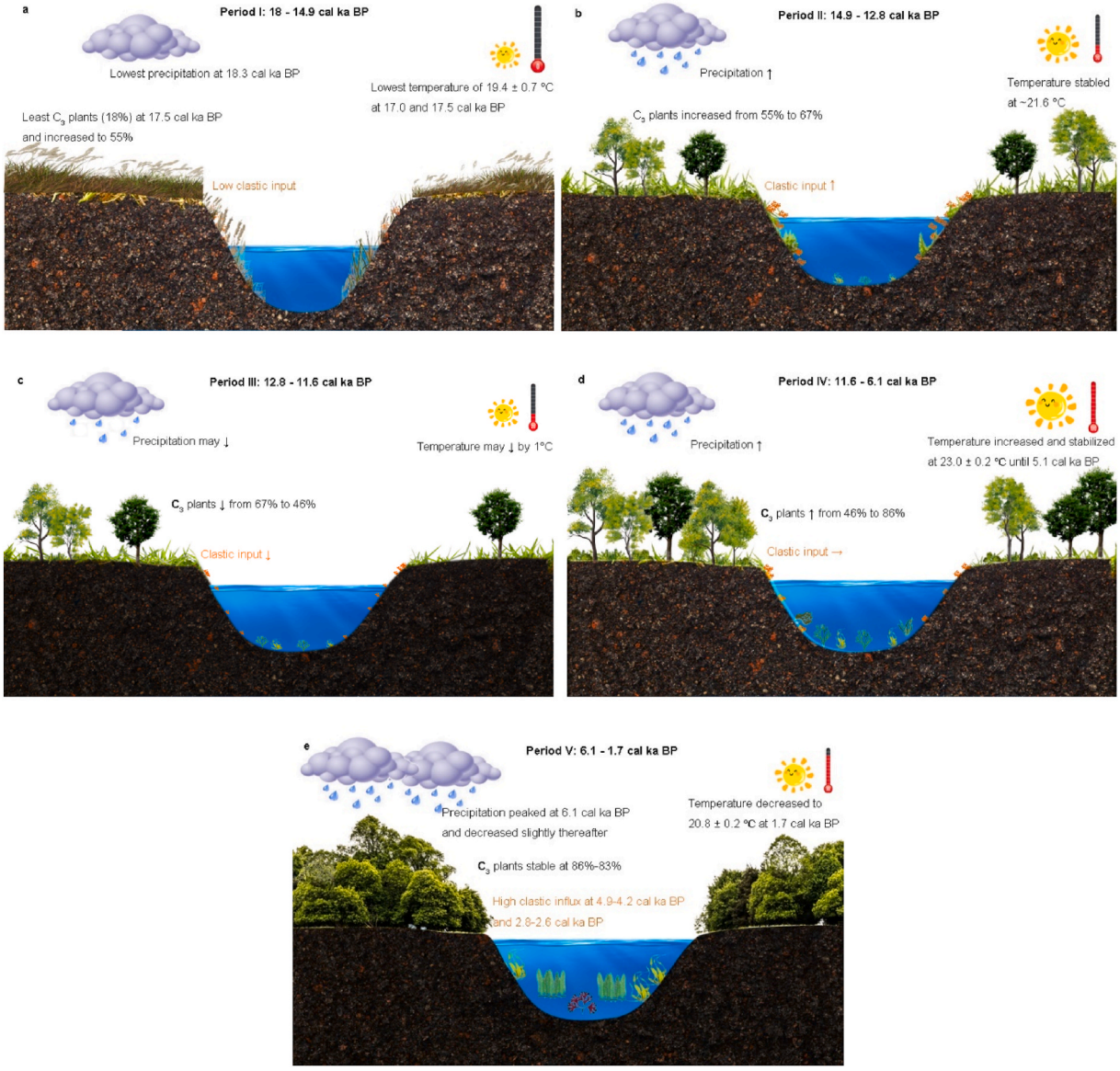

Fig. 7. Visualization of climatic and environmental changes at Lake Barrine over the period of 18.3–1.7 cal ka BP. The arrows ↑, →, ↓ denote increase, stability, and decrease, respectively.

Antarctic Cold Reversal (14.7–13.0 cal ka BP; Jouzel et al., 1995). From 12.8 to 11.6 cal ka BP, the $\delta^2H_{P\text{-}R}$ value increased to −21.1‰, indicating less rainfall during the period covering the Younger Dryas in this region. From 11.6 to 6.1 cal ka BP, the $\delta^2H_{P\text{-}R}$ value generally decreased and reached the lowest values in the record (−65.5‰) at 6.1 cal ka BP, which suggests increasingly intense monsoonal rainfall into the early and middle Holocene. From 6.1 to 1.7 cal ka BP, the $\delta^2H_{P\text{-}R}$ value fluctuated erratically and overall increased to −53.5‰, suggesting less rainfall and/or more rainfall variability.

4.3. A robust multi-proxy-based record of climate and environmental change at Lake Barrine

The results from this study enable the identification of robust environmental and climatic records of change by combining multiple proxies from the sediment record in Lake Barrine. The proxies include the reconstructed fraction of C_3 plants from $\delta^{13}C$ values of C_{31} *n*-alkane ($\delta^{13}C_{n\text{-}C31}$), the reconstructed δ^2H values of precipitation ($\delta^2H_{P\text{-}R}$) in this study, as well as pollen (Walker, 2007), brGDGTs (Li et al., 2023), clastic and Ti influxes (Ti Itrax counts/accumulation years, modified from Li et al., 2022). The fraction of C_3 plants and pollen enable inferences in relation to vegetation change, the $\delta^2H_{P\text{-}R}$ values indicate changes associated with the relative intensity of monsoonal precipitation, the brGDGTs allow inferences of mean annual air temperature (air temperature hereafter) change, while clastic and Ti influxes suggest the accumulation rate of clastic input into Lake Barrine. The pollen record (Walker, 2007) covers only the past 13.2 kyr whereas all other proxies cover the period from 18.3 to 1.7 cal ka BP.

The period from 18.3 to 17.5 cal ka BP appears to have been relatively dry and cool (Fig. 7a). The $\delta^{13}C_{n\text{-}C31}$ values suggest that the catchment around Lake Barrine was probably mostly covered by grassy open savanna, because C_4 plant biomass is estimated to be over 75–82%

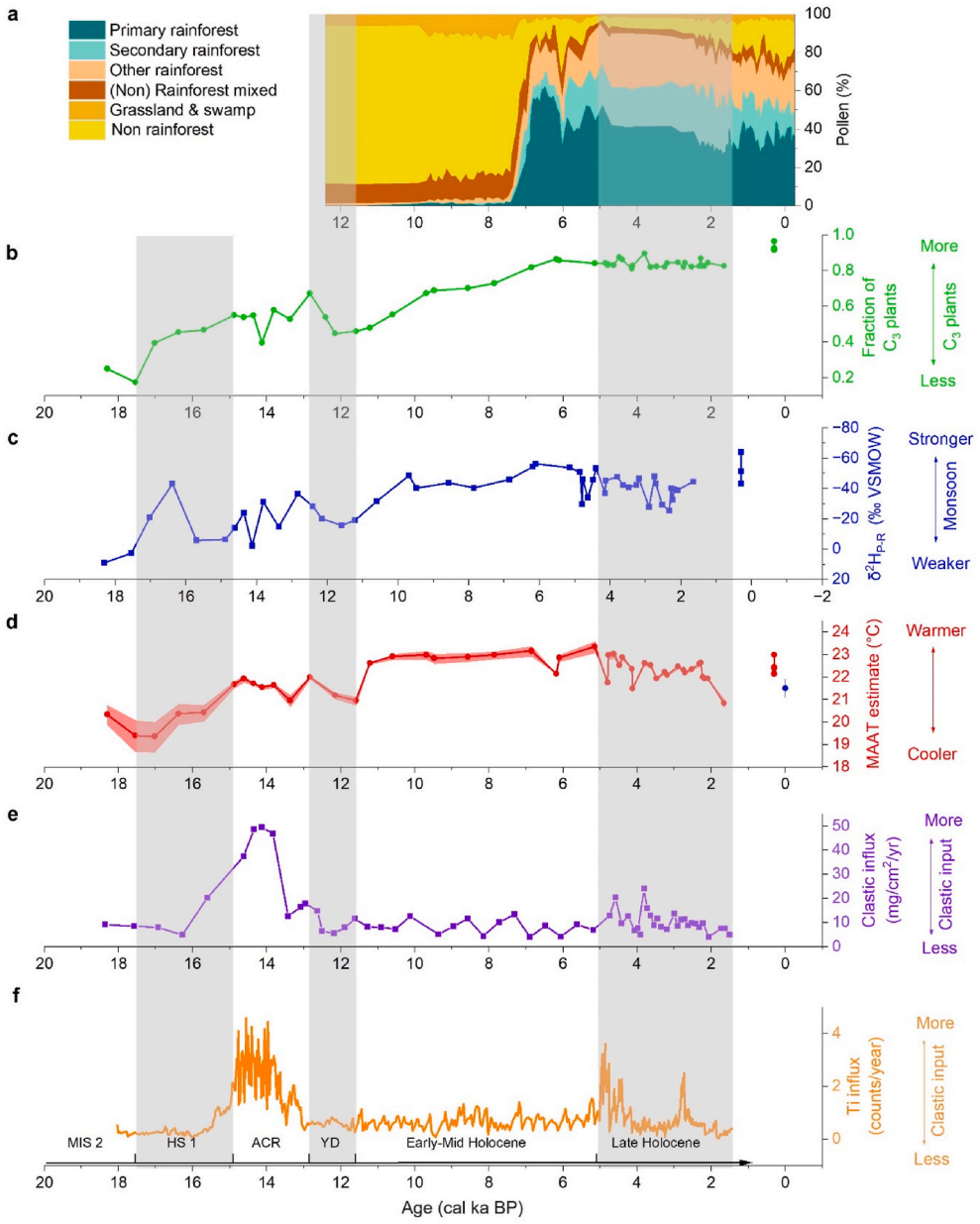

Fig. 8. A selection of representative proxies from Lake Barrine sediment records. a. Pollen record (Walker, 2007); **b.** Reconstructed fraction of C_3 plants (this study); **c.** Reconstructed δ^2H values of precipitation (this study); **d.** Mean annual air temperature estimates (Li et al., 2023) **e.** Clastic influx (Li et al., 2022); **f.** Ti influx (Ti Itrax counts/accumulation years, modified from Li et al., 2022). The three gray vertical bars divide the record into MIS 2 (Marine Isotope Stage 2), HS1 (Heinrich stadial 1), ACR (Antarctic Cold Reversal), YD (Younger Dryas), early-mid Holocene, and late Holocene.

(Fig. 8b). High $\delta^2H_{P\text{-}R}$ values (+5.9‰ to +0.5‰; Fig. 8c) suggest that the monsoon was weak, with low overall precipitation. Increased evaporation (both in soil and leaf water) due to the aridity may have also contributed to the particularly high $\delta^2H_{P\text{-}R}$ values during this period (Kahmen et al., 2013). BrGDGTs from the lake sediment suggest that the annual air temperature was the lowest (19.4 ± 0.7 °C) at 17.5 and 17.0 cal ka BP for the past 18,300 years, 3.1 ± 0.9 °C colder compared to current temperatures (Fig. 8d; Li et al., 2023). The low clastic and Ti influxes suggest low clastic input (Fig. 8e; f; Li et al., 2022), consistent with the low precipitation and savanna cover.

From 17.5 to 14.9 cal ka BP, the proxies below suggest a general trend to wetter and warmer conditions at Lake Barrine compared to the preceding period. The decreasing $\delta^2H_{P\text{-}R}$ values (from +0.5‰ to −12.8‰; Fig. 8c) suggest a progressive increase in monsoon strength bringing more precipitation, especially from 17.0 to 16.4 cal ka BP. The brGDGT record indicates that air temperature increased from 19.4 ± 0.7 °C to 21.9 ± 0.2 °C over the period from 17.0 to 14.6 cal ka BP (Fig. 8d; Li et al., 2023). The $\delta^{13}C_{n\text{-}C31}$ values of the lake sediment suggest that C_3 plants increased from 18% to 55% during this period (Fig. 8b), indicating a progressive increase in woody canopy cover, but no extraordinary changes from 17.0 to 16.4 cal ka BP when $\delta^2H_{P\text{-}R}$ values suggest intensified monsoon. The clastic and Ti influxes were low but started to increase from 15.4 cal ka BP, inferring increasing detrital inputs as a result of more precipitation (Fig. 8e; f).

The period from 14.9 to 12.8 cal ka BP encompasses the Antarctic cold reversal, but the brGDGTs has suggested that air temperature was stable at ~21.6 °C at Lake Barrine (Fig. 8d; Li et al., 2023). The decreasing $\delta^2H_{P\text{-}R}$ values (from −12.8‰ to −44.1‰; Fig. 8c) suggest that the monsoon continued to strengthen, implying a further increase in precipitation compared to earlier in the record. The $\delta^{13}C_{n\text{-}C31}$ values indicate that C_3 plants increased from 55% to 67% (Fig. 8b). This is generally consistent with the pollen record (Walker, 2007) which has suggested dominant shrubs and trees, such as *Allocasuarina*, *Eucalyptus* and *Callitris*, and ~10% grass pollen from 13.2 to 7.4 cal ka BP (Fig. 8a). The clastic influx into the lake peaked from 14.9 to 13.1 cal ka BP (Fig. 8e; f), likely as a result of intense rainfall when the catchment was relatively sparsely covered by grasses and sclerophyll shrubs and trees.

From 12.8 to 11.6 cal ka BP, the proxies below indicate a return to drier and cooler conditions compared to the previous period (Fig. 7c). The $\delta^2H_{P\text{-}R}$ values increased by 21‰ (from −44.1‰ to −21.1‰; Fig. 8c), suggesting less precipitation brought by the Indonesian-Australian summer monsoon. Air temperature at Lake Barrine possibly decreased by ~1.0 °C, but this trend was based only on three samples and the variation is within the root mean square errors (2.1 °C), so that the reliability of this temperature drop is not high (Fig. 8d; Li et al., 2023). The $\delta^{13}C_{n\text{-}C31}$ values indicate that C_3 plants in the catchment decreased marginally from 67% to 46% (Fig. 8b) during this period in response to lower rainfall. This millennial shift was not noted in the pollen records as no samples covering this period were analyzed (Walker, 2007) (Fig. 8a). The low clastic influx into the lake from 13.0 to 11.6 cal ka BP (Fig. 8e; f) is compatible with the decreased rainfall.

From 11.6 to 6.1 cal ka BP, there was a sustained period of increasingly wet and warm conditions compared to the earlier period (Fig. 7d). The $\delta^2H_{P\text{-}R}$ values decreased by −41‰ (−21.1‰ to −65.5‰; Fig. 8c) reaching the lowest value at 6.1 cal ka BP in the past 18,300 years, indicating that the Indonesian-Australian summer monsoon was particularly strong, bringing abundant monsoonal precipitation. The clastic influx remained low from the early to middle Holocene, similar to the previous period (Fig. 8e; f), likely because increasing tree cover reduced the erosive potential of the monsoonal rain in the catchment. The brGDGTs suggest that this was the warmest period over the past 18,300 years with air temperature fluctuating around 23.0 ± 0.2 °C from 11.2 to 5.1 cal ka BP (Fig. 8d; Li et al., 2023). In response to the warm, wet conditions, C_3 plants increased to 86% in the catchment at 6.1 cal ka BP (Fig. 8b). This timing is comparable to the peak time of 6.7 cal ka BP in rainforest pollen (Walker, 2007). The consistency between proxies may indicate that a closed rainforest canopy in the Lake Barrine catchment was established from 7.3 to 6.1 cal ka BP (Walker, 2007; Li et al., 2022).

However, the pollen proportions of different life forms remained stable from 13.2 to 7.3 cal ka BP (Walker, 2007) while the $\delta^{13}C_{n\text{-}C31}$ values suggest increasing C_3 plants during this period (Fig. 8b). Additionally, the pollen record indicates a rapid rainforest expansion from 7.3 to 6.7 cal ka BP (Walker, 2007) while the $\delta^{13}C_{n\text{-}C31}$ values suggest a gradual development of rainforest and non-rainforest trees from 11.6 to 6.1 cal ka BP (Fig. 8b). The difference is likely because the pollen from Lake Barrine records vegetation over a broader area beyond the crater rim, and trees were not well developed due to broadly spread fire events before 7.3 cal ka BP (Walker, 2007; Haberle et al., 2010). After 7.3 cal ka BP, a threshold, likely in rainfall, or seasonality of rainfall, was crossed that enabled the rapid expansion of forest across the broader savanna landscape beyond the Barrine crater, possibly from a refugial population in the crater. In contrast, the $\delta^{13}C_{n\text{-}C31}$ values reflect local vegetation within the catchment itself, and the record indicates a much more gradual increase in tree cover in the catchment itself, in response to the more gradual increase in rainfall suggested by the $\delta^2H_{P\text{-}R}$ record (Fig. 8c).

From 6.1 to 1.7 cal ka BP, there was a trend back toward slightly drier and cooler conditions compared to the previous period (Fig. 7e). The reconstructed C_3 plant abundance remained relatively stable (from 86% to 83%) from 6.1 to 1.7 cal ka BP (Fig. 8b), consistent with the pollen record that has suggested slightly decreased rainforest and increased non-rainforest taxa after 6.7 cal ka BP (Walker, 2007). The $\delta^2H_{P\text{-}R}$ values increased by 12‰ (from −65.5‰ to −53.5‰; Fig. 8c) implying that the intensity of the Indonesian-Australian summer monsoon overall decreased, bringing less rainfall. After 5 cal ka BP, there is a marked increase in inter-sample variability in $\delta^2H_{P\text{-}R}$ values, suggesting increased monsoon variability. This increased variability is also evident in the record of clastic influx (Fig. 8e; f) and air temperature (Fig. 8d), but the fraction of C_3 plants remained stable (Fig. 8b). We therefore consider this variability increase is unlikely to be an artifact of increased sampling resolution, but possibly results from an increased irregularity in El-Niño Southern Oscillation (ENSO) (Moy et al., 2002; Conroy et al., 2008).

In modern days, the $\delta^2H_{P\text{-}R}$ estimate (−59.0 ± 9.2‰; Fig. 8b) and C_3 plant fraction (93 ± 0.02%; Fig. 8c) suggest that the modern intensity of Indonesian-Australian summer monsoon are similar to the conditions at 1.7 cal ka BP while rainforest trees may have increased. The increased rainforest cover is consistent with warmer climate (Li et al., 2023) and higher CO_2 concentration in the atmosphere (Monnin et al., 2004). BrGDGT analysis has indicated that air temperature decreased from 23.0 ± 0.2 °C to 20.8 ± 0.2 °C from 5.1 to 1.7 cal ka BP and increased by 1.6 °C–22.4 ± 0.4 °C at the present time (Fig. 8d; Li et al., 2023).

4.4. Regional environmental change

This section places the record from Lake Barrine in the context of regional records and known major inflections in global climate from the last Glacial to the present. Discussion is therefore organized around known global or Southern Hemisphere periods of environmental change.

4.4.1. The last deglaciation (18.0–14.9 cal ka BP)

Paleoenvironmental records on and near the Atherton Tablelands (Li et al., 2022) consistently suggest a dry and cool climate during this period. In terms of vegetation, the $\delta^{13}C_{n\text{-}C31}$ values of the sediment in Lake Barrine allow us to infer that C_4 plant biomass comprised over 75% of total biomass in the catchment from 18.3 to 17.5 cal ka BP after which time C_3 plants began to increase in representation. Pollen from Lake Euramoo suggests that grasses and sclerophyll woodland taxa dominated (>95% of total pollen) the region and palynological richness was minimal from 23 to 16.8 cal ka BP (Haberle, 2005). Rainforest

gymnosperms *Agathis* and *Podocarpus* first appeared by 15.5 cal ka BP in the pollen record from Lake Euramoo (Haberle, 2005). ODP site 820 records similar vegetation conditions, including reduced woody plants (Cunoniaceae, Myrtaceae) and increased sedges and grasses (Cyperaceae and Poaceae) from 23.7 to 17.2 cal ka BP (Moss et al., 2017), indicating drier conditions in the broad region sampled in the offshore marine core.

The estimated high δ^2H values of precipitation ($\delta^2H_{P\text{-}R}$; $\geq -12.8‰$) at Lake Barrine suggest that the Indonesian-Australian summer monsoon was probably not developed during this period except possibly for a wetter period (−23‰ decrease) from 17.0 to 16.4 cal ka BP. At a similar time in southern China, the Hulu cave stalagmite records a sharp ca. 2‰ increase in $\delta^{18}O$ values (16.1 ± 0.06 ka BP), indicating a drier period in the East Asian summer monsoon region more broadly (Wang, 2001). From 17.0 to 16.0 ka BP, the $\delta^{18}O$ values of stalagmite decreased by −4‰ in Ball Gown Cave in northwestern Australia, suggesting a wetter period in that region (Denniston et al., 2013). The anti-phased rainfall distribution in the Indonesian-Australian and East Asian summer monsoon regions may support the speculations that precipitation variations in these regions are correlated and related to movements of the Intertropical Convergence Zone (Li et al., 2022).

In terms of temperature, Lake Barrine records a deglacial warming of 2.5 ± 0.9 °C from 18.0 ± 0.4 to 14.9 ± 0.4 cal ka BP relative to the Last Glacial Maximum (Li et al., 2023). At site 820, the increased foraminiferal $\delta^{18}O$ values (−0.98‰) have been used to infer a cooler climate at 17.2 cal ka BP, after which time, temperature increased until 13.9 cal ka BP (Peerdeman and Chivas, 1993; Moss et al., 2017). In Lynch's Crater, low Cyperaceae, increasing optical absorption values, which was interpreted as increased humification, and reduced organic carbon percentage have been taken to indicate drier conditions from ca. 19.1 to 13.9 cal ka BP (Turney et al., 2006). Additionally, low charcoal amounts in Lake Euramoo and site 820 indicate infrequent fires during this period (Haberle, 2005; Moss et al., 2017), possibly as a result of relatively low biomass available to burn.

4.4.2. The Antarctic cold reversal (14.9–12.8 cal ka BP)

The climatic records on and near the Atherton Tablelands (Turney et al., 2004, 2006; Haberle, 2005; Walker, 2007; Moss et al., 2017) consistently suggest wetter and warmer conditions compared to the preceding period, supporting the conclusion of Li et al. (2022) and this study. This period coincides with the Antarctic cold reversal in the Southern Hemisphere and the Bølling-Allerød warming in the Northern Hemisphere, during which periods temperature decreased in both Hemispheres, even though they have opposite names (Johnsen et al., 1992; Jouzel et al., 1995). The mean annual air temperature at Lake Barrine has been suggested to be stable at ~21.6 °C from 14.9 to 12.8 cal ka BP (Li et al., 2023). The $\delta^2H_{P\text{-}R}$ estimates in this study suggest more rainfall brought by the Indonesian-Australian summer monsoon during this period consistent with the dramatic increase in clastic input during this period when closed forest had not yet developed (Li et al., 2022). Similarly, slightly lower optical absorption values and sharply increased Cyperaceae in the sediment in Lynch's Crater suggest a wetter period from 13.9 to 11.6 cal ka BP (Turney et al., 2004, 2006).

The $\delta^{13}C_{n\text{-}C31}$ values of the sediment in Lake Barrine suggest that C_3 plants increased from 55% to 67% from 14.9 to 12.8 cal ka BP. In terms of vegetation, pollen from Lake Barrine has indicated a regional sparse cover of grasses, and sclerophyllous trees and shrubs from 13.2 (maximum age reported) to 7.4 cal ka BP (Walker, 2007). In Lake Euramoo, the pollen record suggests 10–20% pollen of rainforest taxa from 16.8 to 11.5 cal ka BP, and fine charcoal particles have been used to infer that regional and local grasses probably dominated the fire events from 16.8 to 8.7 cal ka BP (Haberle, 2005). At site 820, pollen with limited resolution (three data points in this period) displays decreased sclerophyll herbs (73%–59%) and increased sclerophyll arboreal taxa (11%–21%) and rainforest angiosperms (6%–12%) (Moss et al., 2017). These paleo-ecological records are generally consistent with the C_3 plant abundance and $\delta^2H_{P\text{-}R}$ estimates in this study, but the timings of the changes are different as described above. These discrepancies may reflect real difference in vegetation conditions, but could also arise from the different sample resolutions and dating uncertainties of the records.

4.4.3. The Younger Dryas (12.8–11.6 cal ka BP)

The record from Lake Barrine indicates this period likely saw a return to drier and cooler conditions compared to the previous period, different from the interpretation of several other records in the region (Turney et al., 2006; Ayliffe et al., 2013; Li et al., 2022). At Lake Barrine, the mean annual air temperature potentially decreased by ~1.0 °C during this period, but the reliability of this inference is not high due to the small temperature variation and only three available samples in this interval (Li et al., 2023). The reconstructed C_3 plant abundance decreased to 46% and the $\delta^2H_{P\text{-}R}$ values increased by 23‰ during this period, suggesting decreased monsoonal rainfall. No pollen samples were analyzed in Lake Barrine during this period due to limited sampling resolution (Walker, 2007). In Lake Euramoo, the pollen record indicates that rainforest gymnosperms disappeared from 12.6 to 9.6 cal ka BP; instead, dry sclerophyll taxa (mainly *Casuarina*) dominated between 11.5 and 9.6 cal ka BP, also suggestive of drier conditions (Haberle, 2005). Notably, the reliability of this pollen climate reconstruction for this period is not high because only three samples were analyzed (Haberle, 2005).

Turney et al. (2006) has interpreted the period from ca. 12.6 to 11.6 cal ka BP as one of significant moisture availability due to increased carbon content and a spike in monolete fern spores in Lynch's Crater. However, increasing optical absorption values indicated a drier climate during this period, but the optical absorption was considered less sensitive due to the inconsistency associated with the high carbon content (Turney et al., 2006). Nonetheless, both lower clastic input (suggestive of dry or wet conditions) and higher organic carbon input (suggestive of wet conditions) can result in a higher carbon content. Taking these elements into consideration, it is therefore possible that Lynch's Crater recorded drier climate during this period.

Similarly, Li et al. (2022) has suggested this period to be wetter because of increased C:N ratios (21) and lower $\delta^{13}C$ values of bulk organic carbon ($\delta^{13}C_{TOC}$; −28.6‰) in the sediment in Lake Barrine. However, these two proxies reflect both terrestrial and aquatic plant inputs and the changes observed could have been driven by changes in the proportion of aquatic-derived carbon in this period. The $\delta^{13}C_{n\text{-}C31}$ and $\delta^2H_{n\text{-}C31}$ values are more specific and reliable indicators of the terrestrial environment than the bulk proxies used by Li et al. (2022). Thus, the indications of decreased C_3 plant percentage and lower precipitation derived from the $\delta^{13}C_{n\text{-}C31}$ and $\delta^2H_{n\text{-}C31}$ values are considered to be more robust.

4.4.4. Early to middle Holocene (11.6–5 cal ka BP)

The reconstructed $\delta^2H_{P\text{-}R}$ values at Lake Barrine suggest that the monsoon brought progressively more precipitation during this period compared to prior conditions, with maximum precipitation inferred at 6.1 cal ka BP. In Lynch's crater, Turney et al. (2006) has suggested a drier shift between ca. 11.6 to 10.9 cal ka BP followed by a shift to wetter conditions thereafter to 10 cal ka BP (the uppermost interval reported) based on pollen amount of *Cyperaceae* and *Poaceae*, and monolete fern spores. However the optical absorption values of the peat changed little from 11.6 to 10 cal ka BP (Turney et al., 2006), suggesting little variation in moisture availability at that time.

The $\delta^{13}C_{n\text{-}C31}$ values of the sediment in Lake Barrine suggest that C_3 plants in the catchment reached the highest abundance (86%) at 6.1 cal ka BP except for the modern day. Pollen from Lake Barrine has indicated regionally and locally dominant non-rainforest trees and shrubs and grassland components from 13.2 to 7.4 cal ka BP, after which time the representation of rainforest taxa in the pollen record rapidly peaked over a few centuries at 6.7 cal ka BP (Walker, 2007). In Lake Euramoo, pollen indicates a regional and local shift from sclerophyll to a warm

temperate rainforest dominance from 8.7 to 5.0 cal ka BP, with the pollen of rainforest taxa sharply rising to ~80–90% at 7.3 cal ka BP (Haberle, 2005). Rainforest taxa attained maximum percentage (close to 100%) at 6.3 cal ka BP (Haberle, 2005), similar to the pollen record in Lake Barrine (Walker, 2007). Charcoal influx reached a minimum between ca. 7.3 to 6.3 cal ka BP when the rainforest taxa reached the maximum at Lake Euramoo (Haberle, 2005). At ODP site 820, pollen suggests a sharp increase in major complex rainforest taxa and fern spores, and reduced sclerophyll canopy from ca. 9.5 to 8.5 cal ka BP (Moss et al., 2017), also implying warmer and wetter conditions. There is agreement between multiple lines of evidence from multiple sites, including Lake Barrine, that the wettest and warmest conditions in the Holocene occurred in this period, with minor differences in the timing of peak wet conditions.

4.4.5. Late Holocene (5 cal ka BP–the present)

On the Tablelands, this period saw drying and cooling conditions relative to the early and middle Holocene. The brGDGT record from the sediment in Lake Barrine indicates that air temperature decreased from 23.0 ± 0.2 °C to 20.8 ± 0.2 °C from 5.1 to 1.7 cal ka BP (Li et al., 2023). The increased $\delta^2H_{P\text{-}R}$ values (by 9‰) implies some decrease in the intensity of the Indonesian-Australian summer monsoon, bringing less rainfall from 6.1 to 1.7 cal ka BP. The reconstructed C_3 plant percentage around Lake Barrine remained relatively stable (86%–83%) from 6.1 to 1.7 cal ka BP. The pollen record from the lake suggests slightly decreased rainforest and increased non-rainforest taxa in the broader region after 6.7 cal ka BP, especially with a rise in non-rainforest pollen from 2.2 to 0.3 cal ka BP (Walker, 2007), consistent with the geochemical indicators. In Lake Euramoo, pollen indicates a dry subtropical rainforest, represented by Elaeocarpaceae, *Agathis* and *Trema*, that dominated from 5.0 to 0.07 cal ka BP in this region (Haberle, 2005). At ODP site 820, pollen displays a decrease in rainforest taxa and an increase in sclerophyll herbs from 8.5 cal ka BP to the present across the broad catchment area of this marine core (Moss et al., 2017).

Fire events, clastic input, and sediment accumulation rate in specific lakes are also included to form a comprehensive picture of environmental and climatic changes on the Tablelands. Fine and coarse charcoal particles were present in the sediment in Lake Euramoo from 5.0 to 0.07 cal ka BP, with a series of peaks from 4.0 cal ka BP onwards (Haberle, 2005), suggesting increasing fire events in the late Holocene. Lake Barrine recorded two clastic influx peaks during periods from 4.9 to 4.2 cal ka BP and from 2.8 to 2.6 cal ka BP; meanwhile, the $\delta^2H_{P\text{-}R}$ values increased by ~23‰ but the $\delta^{13}C_{n\text{-}C31}$ values remained stable. Interestingly, Lake Euramoo also records a rise in sediment accumulation rate between 2.7 and 1.2 cal ka BP (Haberle, 2005), at a similar time to the clastic influx increase in Lake Barrine. We consider these variations may be related to higher variability in precipitation, possibly related to increased ENSO variability as observed in other regional records (Moy et al., 2002; Conroy et al., 2008; Toth and Aronson, 2019; Tan et al., 2020).

According to the modern surface sediment samples, the average δ^2H estimate of precipitation (−59.0 ± 9.2‰) and C_3 plant fraction (93 ± 0.02%) suggest that the monsoon intensity may be like the conditions at 1.7 cal ka BP but C_3 plants have increased further at Lake Barrine. On the other hand, the pollen from this lake records that non-rainforest pollen, particularly *Allocasuarina*, decreased to ca. 10% after 300 cal a BP (Walker, 2007). The pollen from Lake Euramoo indicates that sclerophyll taxa maintained at low values whereas several rainforest taxa declined markedly, most likely due to selective logging in the 19th century (Haberle, 2005). Charcoal particle accumulation rate in this lake returned to high values from 1880 to 1999 CE, comparable with values in the early Holocene (Haberle, 2005), indicating more frequent fire events in recent times.

5. Conclusions

In this study, we analyzed *n*-alkanes from modern plants and a sedimentary record to study the climate and vegetation change since 18.3 cal ka BP in tropical northeastern Australia. We firstly investigated the relationships of relative distributions, carbon and hydrogen isotope compositions of long-chain *n*-alkanes from modern biomass, leaf litter, soils, and surface sediments from Lake Barrine. Based on this comparison, we developed a vegetation composition model to estimate C_3 plant fraction and a vegetation-corrected precipitation model ($\delta^2H_{P\text{-}R}$) to enable tracking monsoon intensity at this lake over time. Lastly, combining the results in this study with air temperature (Li et al., 2023), pollen (Walker, 2007), and clastic influxes (Li et al., 2022), we built a robust climatic and environmental record at Lake Barrine and compared it with other paleoenvironmental records from the region. The main conclusions are as follows:

The average fractional abundances of C_{23}–C_{35} *n*-alkanes indicate that *n*-C_{31} dominates in all sample types at this tropical site, including modern rainforest tree leaves, grasses, fallen leaves, soils, and lake sediments. The fractional abundances of *n*-C_{28}, *n*-C_{29}, *n*-C_{30} decreased while that of *n*-C_{31} remained unchanged and *n*-C_{33} increased in soil samples compared to *in situ* fallen leaves. Slight ^{13}C enriching and obvious ^2H depleting trends are seen in the *n*-C_{31} (same for *n*-C_{29} and *n*-C_{33}) from the fresh rainforest leaves, rainforest fallen leaf mixture, catchment soils, and surface sediments. The changed fractional abundances, slightly enriched ^{13}C, and obviously depleted ^2H in *n*-alkanes suggest possible microbial *n*-alkane build-up during decomposition and/or diagenesis.

The modern C_3 vegetation is estimated to be 93% using the vegetation composition model, close to the observed number of ~100%. We therefore infer that the C_3 plant fraction estimates in the catchment over time are impacted little by the slight ^{13}C enrichment during terrestrial decomposition process. By contrast, the δ^2H estimates of modern precipitation using surface sediments is −22‰ lower than the measured δ^2H values of precipitation around Lake Barrine. The terrestrial ^2H depletion in the *n*-C_{31} from fresh rainforest leaves to soils, −19‰, offsets the −22‰ difference, suggesting that *n*-alkanes from soils represent better end members for use in the vegetation-corrected precipitation model.

In the downcore sediments, as the trends for the $\delta^{13}C$ and δ^2H values of the *n*-C_{29}, *n*-C_{31} and *n*-C_{33} in the sediments are similar, we present the results of vegetation and precipitation changes using the most abundant component *n*-C_{31}. The multiple proxies, $\delta^{13}C_{n\text{-}C31}$, $\delta^2H_{n\text{-}C31}$ values, pollen (Walker, 2007), air temperature (Li et al., 2023), and clastic influxes (Li et al., 2022), from Lake Barrine cross check and are closely correlated with each other, except for an inconsistency from 17.0 to 16.4 cal ka BP when two low $\delta^2H_{P\text{-}R}$ values suggest wetter conditions while no variations occurred in clastic influx or C_3 plant percentage.

A broad consistency was identified between the robust paleoclimatic record developed from Lake Barrine and other paleoenvironmental records on the Atherton Tablelands. The records on the Tablelands include pollen in Lake Barrine, Lake Euramoo, Lynch's Crater and ODP site 820, and other less commonly applied proxies including optical absorption and Ti from these sites. The consistency between results across the broader suite of studies include cool, dry Last Glacial Maximum (23–17.0 cal ka BP), warmer, wetter last deglacial (17.0–14.9 cal ka BP), stable temperature, wetter Antarctic cold reversal (14.9–12.8 cal ka BP), (possibly) cooler, drier Younger Dryas (12.8–11.6 cal ka BP), warmer, wetter early-to-middle Holocene (11.6–5 cal ka BP) and cooler, slightly drier and more variable late Holocene (5 cal ka BP to the present).

Author Contributions

Conceptualization: Michael I. Bird, Chris M. Wurster, Ting Li, Methodology: Chris M. Wurster, Ting Li, Youping Zhou, Software: Ting Li, Investigation: Ting Li, Xiuwen Zhou, Youping Zhou, Yu Zhao, Rainy

Comley, Jordahna Haig, Resources: Youping Zhou, Niels C. Munksgaard, Lucas A. Cernusak, Writing – original draft: Ting Li, Writing – review & editing: All coauthors

Declaration of competing interest

The authors declare that they have no known competing financial interests or personal relationships that could have appeared to influence the work reported in this paper.

Data availability

All data are included as supplementary tables.

Acknowledgements

The first author would like to thank the lovely teachers and students in the Isotopomics in Chemical Biology Lab (ICB) for the inclusion and help. The first author also thanks Dr. Xennephone Hadeen for showing extracting *n*-alkanes from lake sediments. We thank Raelee Kerrigan, project officer of Australian Tropical Herbarium for identifying the species of the grass samples. This work is contribution #34 from the ICB group. The work was supported by the Australian Research Council Centre of Excellence for Australian Biodiversity and Heritage (CE170100015) and the National Natural Science Foundation of China (Nos. 41973072; 42250203).

Appendix A. Supplementary data

Supplementary data to this article can be found online at https://doi.org/10.1016/j.quascirev.2024.108807.

References

Aichner, B., Herzschuh, U., Wilkes, H., 2010. Influence of aquatic macrophytes on the stable carbon isotopic signatures of sedimentary organic matter in lakes on the Tibetan Plateau. Org. Geochem. 41, 706–718. https://doi.org/10.1016/j.orggeochem.2010.02.002.

Ayliffe, L.K., Gagan, M.K., Zhao, J.-x., Drysdale, R.N., Hellstrom, J.C., Hantoro, W.S., Griffiths, M.L., Scott-Gagan, H., Pierre, E.S., Cowley, J.A., Suwargadi, B.W., 2013. Rapid interhemispheric climate links via the Australasian monsoon during the last deglaciation. Nat. Commun. 4, 2908. https://doi.org/10.1038/ncomms3908.

Bauman, D., Fortunel, C., Cernusak, L.A., Bentley, L.P., McMahon, S.M., Rifai, S.W., Aguirre-Gutierrez, J., Oliveras, I., Bradford, M., Laurance, S.G.W., Delhaye, G., Hutchinson, M.F., Dempsey, R., McNellis, B.E., Santos-Andrade, P.E., Ninantay-Rivera, H.R., Chambi Paucar, J.R., Phillips, O.L., Malhi, Y., 2022. Tropical tree growth sensitivity to climate is driven by species intrinsic growth rate and leaf traits. Glob Chang Biol 28, 1414–1432. https://doi.org/10.1111/gcb.15982.

Bird, M.I., Roger, E., Summons, Michael, K., 1995. Terrestrial vegetation change inferred from n-alkane δ13C analysis in the marine environment. Geochem. Cosmochim. Acta 59, 2853–2857. https://doi.org/10.1016/0016-7037(95)00160-2.

Bird, M.I., Brand, M., Diefendorf, A.F., Haig, J.L., Hutley, L.B., Levchenko, V., Ridd, P.V., Rowe, C., Whinney, J., Wurster, C.M., Zwart, C., 2019. Identifying the 'savanna' signature in lacustrine sediments in northern Australia. Quat. Sci. Rev. 203, 233–247. https://doi.org/10.1016/j.quascirev.2018.11.002.

Blaauw, M., Christen, J.A., 2011. Flexible paleoclimate age-depth models using an autoregressive gamma process. Bayesian Anal. 6, 457–474. https://dx.doi.org/10.1214/11-BA618.

Bore 92678, 92710, 1991. Qeensland Government Groundwater Information.

Bore 148037, 148111, 2009. Qeensland Government Groundwater Information.

Brittingham, A., Hren, M.T., Hartman, G., 2017. Microbial alteration of the hydrogen and carbon isotopic composition of n-alkanes in sediments. Org. Geochem. 107, 1–8. https://doi.org/10.1016/j.orggeochem.2017.01.010.

Chen, Y., 1986. Early Holocene Vegetation Dynamics of Lake Barrine Basin, Northeast Queensland, Australia. Australian National University, Canberra, Australia (PhD thesis).

Chikaraishi, Y., Naraoka, H., 2006. Carbon and hydrogen isotope variation of plant biomarkers in a plant–soil system. Chem. Geol. 231, 190–202. https://doi.org/10.1016/j.chemgeo.2006.01.026.

Conroy, J.L., Overpeck, J.T., Cole, J.E., Shanahan, T.M., Steinitz-Kannan, M., 2008. Holocene changes in eastern tropical Pacific climate inferred from a Galápagos lake sediment record. Quat. Sci. Rev. 27, 1166–1180.

Craig, H., 1961. Isotopic variations in meteoric waters. Science 133, 1702–1703.

Denniston, R.F., Wyrwoll, K.-H., Asmerom, Y., Polyak, V.J., Humphreys, W.F., Cugley, J., Woods, D., LaPointe, Z., Peota, J., Greaves, E., 2013. North Atlantic forcing of millennial-scale Indo-Australian monsoon dynamics during the Last Glacial period. Quat. Sci. Rev. 72, 159–168. https://doi.org/10.1016/j.quascirev.2013.04.012.

Diefendorf, A.F., Freeman, K.H., Wing, S.L., Currano, E.D., Mueller, K.E., 2015. Paleogene plants fractionated carbon isotopes similar to modern plants. Earth Planet Sci. Lett. 429, 33–44. https://doi.org/10.1016/j.epsl.2015.07.029.

Diefendorf, A.F., Freimuth, E.J., 2017. Extracting the most from terrestrial plant-derived n-alkyl lipids and their carbon isotopes from the sedimentary record: a review. Org. Geochem. 103, 1–21. https://doi.org/10.1016/j.orggeochem.2016.10.016.

Diefendorf, A.F., Mueller, K.E., Wing, S.L., Koch, P.L., Freeman, K.H., 2010. Global patterns in leaf 13C discrimination and implications for studies of past and future climate. Proc. Natl. Acad. Sci. USA 107, 5738–5743. https://doi.org/10.1073/pnas.0910513107.

Eglinton, G., Hamilton, R.J., 1967. Leaf epicuticular waxes. Science 156, 1322–1335.

Farquhar, G.D., Ehleringer, J.R., Hubick, K.T., 1989. Carbon isotope discrimination and photosynthesis. Annu. Rev. Plant Biol. 40, 503–537.

Feakins, S.J., 2013. Pollen-corrected leaf wax D/H reconstructions of northeast African hydrological changes during the late Miocene. Palaeogeogr. Palaeoclimatol. Palaeoecol. 374, 62–71. https://doi.org/10.1016/j.palaeo.2013.01.004.

Garcin, Y., Schwab, V.F., Gleixner, G., Kahmen, A., Todou, G., Séné, O., Onana, J.-M., Achoundong, G., Sachse, D., 2012. Hydrogen isotope ratios of lacustrine sedimentary n-alkanes as proxies of tropical African hydrology: insights from a calibration transect across Cameroon. Geochem. Cosmochim. Acta 79, 106–126. https://doi.org/10.1016/j.gca.2011.11.039.

Haberle, S.G., 2005. A 23,000-yr pollen record from Lake Euramoo, wet tropics of NE Queensland, Australia. Quat. Res. 64, 343–356. https://doi.org/10.1016/j.yqres.2005.08.013.

Haberle, S.G., Rule, S., Roberts, P., Heijnis, H., Jacobsen, G., Turney, C., Cosgrove, R., Ferrier, A., Moss, P., Mooney, S., 2010. Paleofire in the wet tropics of northeast Queensland, Australia. PAGES News 18, 78–80.

Hattersley, P.W., 1983. The distribution of C 3 and C 4 grasses in Australia in relation to climate. Oecologia 57, 113–128.

Hayes, J.M., Freeman, K.H., Popp, B.N., Hoham, C.H., 1990. Compound-specific isotopic analyses: a novel tool for reconstruction of ancient biogeochemical processes. Org. Geochem. 16, 1115–1128.

Huang, Y., Dupont, L., Sarnthein, M., Hayes, J.M., Eglinton, G., 2000. Mapping of C4 plant input from north west africa into north east atlantic sediments. Geochem. Cosmochim. Acta 64, 3505–3513. https://doi.org/10.1016/S0016-7037(00)00445-2.

Jardine, F., 1925. The drainage of the Atherton tableland. Trans. R. Geogr. Soc. Australasia (Qld) 1, 131–148.

Jetter, R., Schäffer, S., Riederer, M., 2000. Leaf cuticular waxes are arranged in chemically and mechanically distinct layers: evidence from Prunus laurocerasus L. Plant Cell Environ. 23, 619–628. https://doi.org/10.1046/j.1365-3040.2000.00581.x.

Johnsen, S.J., Clausen, H.B., Dansgaard, W., Fuhrer, K., Gundestrup, N., Hammer, C.U., Iversen, P., Jouzel, J., Stauffer, B., steffensen, J.P., 1992. Irregular glacial interstadials recorded in a new Greenland ice core. Nature 359, 311–313. https://doi.org/10.1038/359311a0.

Jouzel, J., Vaikmae, R., Petit, J.R., Martin, M., Duclos, Y., Stievenard, M., Lorius, C., Toots, M., Mélières, M.A., Burckle, L.H., Barkov, N.I., Kotlyakov, V.M., 1995. The two-step shape and timing of the last deglaciation in Antarctica. Clim. Dynam. 11, 151–161. https://doi.org/10.1007/BF00223498.

Kahmen, A., Hoffmann, B., Schefuß, E., Arndt, S.K., Cernusak, L.A., West, J.B., Sachse, D., 2013. Leaf water deuterium enrichment shapes leaf wax n-alkane δD values of angiosperm plants II: observational evidence and global implications. Geochem. Cosmochim. Acta 111, 50–63. https://doi.org/10.1016/j.gca.2012.09.004.

Koch, K., Ensikat, H.J., 2008. The hydrophobic coatings of plant surfaces: epicuticular wax crystals and their morphologies, crystallinity and molecular self-assembly. Micron 39, 759–772. https://doi.org/10.1016/j.micron.2007.11.010.

Konecky, B., Russell, J., Bijaksana, S., 2016. Glacial aridity in central Indonesia coeval with intensified monsoon circulation. Earth Planet Sci. Lett. 437, 15–24. https://doi.org/10.1016/j.epsl.2015.12.037.

Li, T., Comley, R., Zhang, E., Zhou, Y., Zhou, X., Munksgaard, N.C., Zhu, Z., Haig, J., Zheng, F., Bird, M.I., 2023. Paleo-temperature inferred from brGDGTs over the past 18 cal ka BP from Lake Barrine, tropical NE Australia. Quat. Sci. Rev. 310, 108125 https://doi.org/10.1016/j.quascirev.2023.108125.

Li, T., Wurster, C.M., Haig, J., Zhou, Y., Zwart, C., Ren, J., Comley, R., Munksgaard, N.C., Gadd, P.S., Bird, M.I., 2022. Environmental change inferred from multiple proxies from an 18 cal ka BP sediment record, Lake Barrine, NE Australia. Quat. Sci. Rev. 294, 107751 https://doi.org/10.1016/j.quascirev.2022.107751.

Lisiecki, L.E., Raymo, M.E., 2005. A Pliocene-Pleistocene stack of 57 globally distributed benthic δ18O records. Paleoceanography 20, PA1003. https://doi.org/10.1029/2004PA001071.

Liu, J., An, Z., 2018. A hierarchical framework for disentangling different controls on leaf wax δDn-alkane values in terrestrial higher plants. Quat. Sci. Rev. 201, 409–417. https://doi.org/10.1016/j.quascirev.2018.10.026.

Liu, J., An, Z., 2019. Variations in hydrogen isotopic fractionation in higher plants and sediments across different latitudes: implications for paleohydrological reconstruction. Sci. Total Environ. 650, 470–478. https://doi.org/10.1016/j.scitotenv.2018.09.047.

Liu, J., An, Z., 2020. Leaf wax n-alkane carbon isotope values vary among major terrestrial plant groups: different responses to precipitation amount and temperature, and implications for paleoenvironmental reconstruction. Earth Sci. Rev. 202, 103081 https://doi.org/10.1016/j.earscirev.2020.103081.

Liu, J., Zhao, J., He, D., Huang, X., Jiang, C., Yan, H., Lin, G., An, Z., 2022. Effects of plant types on terrestrial leaf wax long-chain n-alkane biomarkers: implications and

paleoapplications. Earth Sci. Rev. 235, 104248 https://doi.org/10.1016/j.earscirev.2022.104248.
Malanda Alert Station, 2021. Monthly rainfall, 2000-2021, 2021st. Bureau of Meteorology. http://www.bom.gov.au/jsp/ncc/cdio/weatherData/av?p_nccObsCode=139&p_display_type=dataFile&p_stn_num=031183.
McCarroll, D., Loader, N.J., 2004. Stable isotopes in tree rings. Quat. Sci. Rev. 23, 771–801. https://doi.org/10.1016/j.quascirev.2003.06.017.
Metcalfe, D., Liddell, M.J., Bradford, M.G., Green, P.T., 2014. Tropical rainforests of eastern Australia. In: Lindenmayer, D., B, E., Thurgate, N., Lowe, A. (Eds.), Biodiversity and Environmental Change: Monitoring, Challenges and Direction. CSIRO Publishing, Canberra, pp. 111–165.
Monnin, E., Steig, E.J., Siegenthaler, U., Kawamura, K., Schwander, J., Stauffer, B., Stocker, T.F., Morse, D.L., Barnola, J.-M., Bellier, B., 2004. Evidence for substantial accumulation rate variability in Antarctica during the Holocene, through synchronization of CO2 in the Taylor Dome, Dome C and DML ice cores. Earth Planet Sci. Lett. 224, 45–54.
Moss, P.T., Dunbar, G.B., Thomas, Z., Turney, C., Kershaw, A.P., Jacobsen, G.E., 2017. A 60 000-year record of environmental change for the Wet Tropics of north-eastern Australia based on the ODP 820 marine core. J. Quat. Sci. 32, 704–716. https://doi.org/10.1002/jqs.2977.
Moy, Christopher, Seltzer, M., Geoffrey, O., ll, R.d., Donald, T., Anderson, 2002. Variability of El niño/southern oscillation activity at millennial timescales during the Holocene epoch. Nature 420, 162–165.
Munksgaard, N.C., Wurster, C.M., Bass, A., Bird, M.I., 2012. Extreme short-term stable isotope variability revealed by continuous rainwater analysis. Hydrol. Process. 26, 3630–3634.
Munksgaard, N.C., Wurster, C.M., Bird, M.I., 2011. Continuous analysis of delta(1)(8)O and deltaD values of water by diffusion sampling cavity ring-down spectrometry: a novel sampling device for unattended field monitoring of precipitation, ground and surface waters. Rapid Commun. Mass Spectrom. 25, 3706–3712. https://doi.org/10.1002/rcm.5282.
Neldner, V.J., Niehus, R.E., Wilson, B.A., McDonald, W.J.F., Ford, A.J., Accad, A., 2023. The vegetation of Queensland. Descriptions of broad vegetation groups. Queensland Herbarium and Biodiversity Science. Department of Environment and Science, Version 6.0.
Nguyen Tu, T.T., Derenne, S., Largeau, C., Bardoux, G., Mariotti, A., 2004. Diagenesis effects on specific carbon isotope composition of plant n-alkanes. Org. Geochem. 35, 317–329. https://doi.org/10.1016/j.orggeochem.2003.10.012.
Niedermeyer, E.M., Sessions, A.L., Feakins, S.J., Mohtadi, M., 2014. Hydroclimate of the western indo-pacific warm pool during the past 24,000 years. Proc. Natl. Acad. Sci. USA 111, 9402–9406. https://doi.org/10.1073/pnas.1323585111.
O'Leary, M.H., 1981. Carbon isotopic fractionation in plants. Phytochemistry 20, 553–567.
Peerdeman, F.M., Chivas, A.R., 1993. The stable oxygen isotope signal in shallow-water, upper-slope sediments off the Great Barrier Reef (Hole 820A). Proc. Ocean Drill. Progr. Sci. Results 133, 163–173.
Ruiz Pessenda, L.C., De Oliveira, P.E., Mofatto, M., de Medeiros, V.B., Francischetti Garcia, R.J., Aravena, R., Bendassoli, J.A., Zuniga Leite, A., Saad, A.R., Lincoln Etchebehere, M., 2009. The evolution of a tropical rainforest/grassland mosaic in southeastern Brazil since 28,000 14C yr BP based on carbon isotopes and pollen records. Quat. Res. 71, 437–452. https://doi.org/10.1016/j.yqres.2009.01.008.
Russell, J.M., Vogel, H., Konecky, B.L., Bijaksana, S., Huang, Y., Melles, M., Wattrus, N., Costa, K., King, J.W., 2014. Glacial Forcing of Central Indonesian Hydroclimate since 60,000 Y B.P, vol. 111. Proceedings of the National Academy of Sciences, pp. 5100–5105. https://doi.org/10.1073/pnas.1402373111.
Sachse, D., Billault, I., Bowen, G.J., Chikaraishi, Y., Dawson, T.E., Feakins, S.J., Freeman, K.H., Magill, C.R., McInerney, F.A., van der Meer, M.T.J., Polissar, P., Robins, R.J., Sachs, J.P., Schmidt, H.-L., Sessions, A.L., White, J.W.C., West, J.B., Kahmen, A., 2012. Molecular paleohydrology: interpreting the hydrogen-isotopic composition of lipid biomarkers from photosynthesizing organisms. Annu. Rev. Earth Planet Sci. 40, 221–249. https://doi.org/10.1146/annurev-earth-042711-105535.
Sachse, D., Radke, J., Gleixner, G., 2004. Hydrogen isotope ratios of recent lacustrine sedimentary n-alkanes record modern climate variability. Geochem. Cosmochim. Acta 68, 4877–4889. https://doi.org/10.1016/j.gca.2004.06.004.
Schönherr, J., 1982. Resistance of plant surfaces to water loss: transport properties of cutin, suberin and associated lipids. In: Lange, O.L., Nobel, P.S., Osmond, C.B., Ziegler, H. (Eds.), Physiological Plant Ecology II: Water Relations and Carbon Assimilation. Springer Berlin Heidelberg, Berlin, Heidelberg, pp. 153–179.
Schönherr, J., 2000. Calcium chloride penetrates plant cuticles via aqueous pores. Planta 212, 112–118. https://doi.org/10.1007/s004250000373.
Schrag, D.P., Hampt, G., Murray, D.W., 1996. Pore fluid constraints on the temperature and oxygen isotopic composition of the glacial ocean. Science 272, 1930–1932. https://doi.org/10.1126/science.272.5270.1930.
Scroxton, N., Gagan, M.K., Ayliffe, L.K., Hantoro, W.S., Hellstrom, J.C., Cheng, H., Edwards, R.L., Zhao, J.X., Suwargadi, B.W., Rifai, H., 2022. Antiphase response of the Indonesian-Australian monsoon to millennial-scale events of the last glacial period. Sci. Rep. 12, 20214 https://doi.org/10.1038/s41598-022-21843-8.
Sessions, A.L., Burgoyne, T.W., Schimmelmann, A., Hayes, J.M., 1999. Fractionation of hydrogen isotopes in lipid biosynthesis. Org. Geochem. 30, 1193–1200.
Shackleton, N.J., 2000. The 100,000-year ice-age cycle identified and found to lag temperature, carbon dioxide, and orbital eccentricity. Science 289, 1897–1902. https://doi.org/10.1126/science.289.5486.1897.
Shanahan, T.M., McKay, N.P., Hughen, K.A., Overpeck, J.T., Otto-Bliesner, B., Heil, C.W., King, J., Scholz, C.A., Peck, J., 2015. The time-transgressive termination of the african humid period. Nat. Geosci. 8, 140–144. https://doi.org/10.1038/ngeo2329.
Suppiah, R., 1992. The Australian summer monsoon: a review. Prog. Phys. Geogr. 16, 283–318.
Tan, L., Li, Y., Wang, X., Cai, Y., Lin, F., Cheng, H., Ma, L., Sinha, A., Edwards, R.L., 2020. Holocene monsoon change and abrupt events on the western Chinese loess plateau as revealed by accurately dated stalagmites. Geophys. Res. Lett. 47, e2020GL090273 https://doi.org/10.1029/2020gl090273.
Timms, B., 1976. Morphology of lakes barrine. Eacham and Euramoo, Atherton Tableland, north Queensland, Proceedings of the Royal Society of Queensland 81–84.
Toth, L.T., Aronson, R.B., 2019. The 4.2 ka event, ENSO, and coral reef development. Clim. Past 15, 105–119.
Tracey, J.G., 1982. The Vegetation of the Humid Tropical Region of North Queensland. CSIRO, Melbourne.
Turney, C.S.M., Kershaw, A.P., Clemens, S.C., Branch, N., Moss, P.T., Keith Fifield, L., 2004. Millennial and orbital variations of El Nino/Southern Oscillation and high-latitude climate in the last glacial period. Nature 428, 306–310. https://doi.org/10.1038/nature02386.
Turney, C.S.M., Kershaw, A.P., Lowe, J.J., van der Kaars, S., Johnston, R., Rule, S., Moss, P., Radke, L., Tibby, J., McGlone, M.S., 2006. Climatic variability in the southwest pacific during the last termination (20–10 kyr BP). Quat. Sci. Rev. 25, 886–903.
Vimeux, F., Masson, V., Delaygue, G., Jouzel, J., Petit, J.R., Stievenard, M., 2001. A 420,000 year deuterium excess record from East Antarctica: information on past changes in the origin of precipitation at Vostok. J. Geophys. Res. Atmos. 106, 31863–31873. https://doi.org/10.1029/2001JD900076.
Vogts, A., Moossen, H., Rommerskirchen, F., Rullkötter, J., 2009. Distribution patterns and stable carbon isotopic composition of alkanes and alkan-1-ols from plant waxes of African rain forest and savanna C3 species. Org. Geochem. 40, 1037–1054. https://doi.org/10.1016/j.orggeochem.2009.07.011.
Walkamin Research Station, 2021a. Daily maximum temperature 1968-2021. Bureau of Meteorology. http://www.bom.gov.au/jsp/ncc/cdio/weatherData/av?p_nccObsCode=122&p_display_type=dailyDataFile&p_stn_num=031108&p_startYear=.
Walkamin Research Station, 2021b. Daily minimum temperature 1968-2021. Bureau of Meteorology. http://www.bom.gov.au/jsp/ncc/cdio/weatherData/av?p_nccObsCode=123&p_display_type=dailyDataFile&p_stn_num=031108&p_startYear=.
Walker, D., 1999. The characteristics and source of laminated mud at Lake Barrine, Northeast Australia. Quat. Sci. Rev. 18, 1597–1624.
Walker, D., 2007. Holocene sediments of Lake Barrine, north-east Australia, and their implications for the history of lake and catchment environments. Palaeogeogr. Palaeoclimatol. Palaeoecol. 251, 57–82. https://doi.org/10.1016/j.palaeo.2007.02.025.
Wang, Y., 2001. A high-resolution absolute-dated late Pleistocene monsoon record from Hulu cave, China. Science 294, 2345–2348.
Winter, K., Smith, J.A.C., 1996. An Introduction to Crassulacean Acid Metabolism. Biochemical Principles and Ecological Diversity, Crassulacean Acid Metabolism: Biochemistry, Ecophysiology and Evolution. Springer, pp. 1–13.
Zech, M., Pedentchouk, N., Buggle, B., Leiber, K., Kalbitz, K., Marković, S.B., Glaser, B., 2011. Effect of leaf litter degradation and seasonality on D/H isotope ratios of n-alkane biomarkers. Geochem. Cosmochim. Acta 75, 4917–4928. https://doi.org/10.1016/j.gca.2011.06.006.
Zhao, C., Cheng, J., Wang, J., Yan, H., Leng, C., Zhang, C., Feng, X., Liu, W., Yang, X., Shen, J., 2021. Paleoclimate significance of reconstructed rainfall isotope changes in asian monsoon region. Geophys. Res. Lett. 48, e2021GL092460 https://doi.org/10.1029/2021gl092460.
Zhou, Y., Grice, K., Stuart-Williams, H., Farquhar, G.D., Hocart, C.H., Lu, H., Liu, W., 2010. Biosynthetic origin of the saw-toothed profile in delta(13)C and delta(2)H of n-alkanes and systematic isotopic differences between n-, iso- and anteiso-alkanes in leaf waxes of land plants. Phytochemistry 71, 388–403. https://doi.org/10.1016/j.phytochem.2009.11.009.
Zwart, Costijn, Munksgaard, Niels, Protat, C., Alain, Kurita, Naoyuki, Lambrinidis, 2018. The isotopic signature of monsoon conditions, cloud modes, and rainfall type. Hydrol. Process. 32, 2296–2303.
Zwart, C., 2021. *Weather In a Bottle: towards a North Australian Hydro Climate Record.* (PhD Thesis). James Cook University, Cairns, Australia.